Bai et al. *Zool. Res.* 2022, 43(5): 851−870
https://doi.org/10.24272/j.issn.2095-8137.2022.122

ZR | Zoological Research

Article Open Access

Deficiency of transmembrane AMPA receptor regulatory protein γ-8 leads to attention-deficit hyperactivity disorder-like behavior in mice

Wan-Jun Bai[1,2,#], Xing-Guang Luo[3,#], Bao-Hua Jin[1], Kang-Sheng Zhu[1,4], Wen-Yan Guo[1], Xiao-Que Zhu[1], Xia Qin[1], Zu-Xiao Yang[1], Jiao-Jiao Zhao[1], Si-Ruan Chen[1], Ri Wang[1], Jie Hao[1], Fei Wang[5], Yun Stone Shi[6], De-Zhi Kong[1,*], Wei Zhang[1,*]

[1] *Department of Pharmacology*, *Institution of Chinese Integrative Medicine*, *Key Laboratory of Neural and Vascular Biology*, *Ministry of Education*, *Key Laboratory of New Drug Pharmacology and Toxicology*, *Hebei Medical University*, *Research Unit of Digestive Tract Microecosystem Pharmacology and Toxicology*, *Chinese Academy of Medical Sciences*, *Shijiazhuang*, *Hebei* 050017, *China*

[2] *Department of Pharmacy*, *Hebei General Hospital*, *Shijiazhuang*, *Hebei* 050051, *China*

[3] *Beijing Huilongguan Hospital*, *Peking University Huilongguan School of Clinical Medicine*, *Beijing* 100096, *China*

[4] *Fourth Hospital of Hebei Medical University*, *Shijiazhuang*, *Hebei* 050017, *China*

[5] *Department of Psychiatry*, *Affiliated Nanjing Brain Hospital*, *Nanjing Medical University*, *Nanjing*, *Jiangsu* 210029, *China*

[6] *State Key Laboratory of Pharmaceutical Biotechnology and MOE Key Laboratory of Model Animal for Disease Study*, *Model Animal Research Center*, *Nanjing University*, *Nanjing*, *Jiangsu* 210061, *China*

ABSTRACT

Attention-deficit hyperactivity disorder (ADHD) is a neurodevelopmental disorder prevalent in school-age children. At present, however, its etiologies and risk factors are unknown. Transmembrane α-amino-3-hydroxy-5-methyl-4-isoxazolepropionic acid (AMPA) receptor regulatory protein γ-8 (TARP γ-8, also known as calcium voltage-gated channel auxiliary subunit gamma 8 (CACNG8)) is an auxiliary AMPA receptor (AMPAR) subunit. Here, we report an association between TARP γ-8 and ADHD, whereby adolescent TARP γ-8 knockout (KO) mice exhibited ADHD-like behaviors, including hyperactivity, impulsivity, anxiety, impaired cognition, and memory deficits. Human single-nucleotide polymorphism (SNP) analysis also revealed strong associations between intronic alleles in *CACNG8* genes and ADHD susceptibility. In addition, synaptosomal proteomic analysis revealed dysfunction of the AMPA glutamate receptor complex in the hippocampi of TARP γ-8 KO mice. Proteomic analysis also revealed dysregulation of dopaminergic and glutamatergic transmissions in the prefrontal cortices of TARP γ-8 KO mice. Methylphenidate (MPH), which is commonly used to treat ADHD, significantly rescued the major behavioral deficits and abnormal synaptosomal proteins in TARP γ-8 KO mice. Notably, MPH

Received: 12 June 2022; Accepted: 24 August 2022; Online: 26 August 2022

Foundation items: This research was supported by the National Natural Science Foundation of China (81872848, 81803509), National Major Special Project on New Drug Innovation grant (2018ZX09711001-004-003), CAMS Innovation Fund for Medical Sciences (2019-I2M-5-055), Hebei Natural Science Foundation (H2019206038), National Key R&D Program of China (2019YFA0801603), and Natural Science Foundation of Jiangsu Province (BE2019707)

#Authors contributed equally to this work

*Corresponding authors, E-mail: kongdezhi@hebmu.edu.cn; weizhang@hebmu.edu.cn

significantly reversed the up-regulation of Grik2 and Slc6a3 in the prefrontal cortex. MPH also significantly improved synaptic AMPAR complex function by up-regulating other AMPAR auxiliary proteins in hippocampal synaptosomes. Taken together, our results suggest that TARP γ-8 is involved in the development of ADHD in humans. This study provides a useful alternative animal model with ADHD-like phenotypes related to TARP γ-8 deficiency, which has great potential for the development of new therapies.

Keywords: Attention-deficit hyperactivity disorder; TARP γ-8; Methylphenidate; Proteomics; Phenome-wide association study

INTRODUCTION

Attention-deficit hyperactivity disorder (ADHD) is a heterogeneous neurodevelopmental disease in children, usually manifesting as a chronic and hereditary neurobehavioral disorder with a global prevalence of 5.29% and affecting more males than females (Faraone et al., 2015; Polanczyk et al., 2007; Posner et al., 2020). The core symptoms of ADHD include attention deficits, hyperactivity, and impulsiveness (Posner et al., 2020; Thapar & Cooper, 2016). In children and adolescents, ADHD usually occurs with other neuropsychiatric disorders, such as anxiety, intellectual disability, and major depressive disorder (Sharma & Couture, 2013; Thapar & Cooper, 2016). Thus far, the biological mechanisms underlying ADHD are not well understood, although dysregulation of catecholamine signaling in the prefrontal cortex is implicated in its pathophysiology (Arnsten & Pliszka, 2011; Biederman, 2005; Sharma & Couture, 2013). Methylphenidate (MPH), the first-line drug for ADHD, enhances synaptic dopamine and norepinephrine transmission by blocking presynaptic dopamine and norepinephrine transporters (Posner et al., 2020; Sharma & Couture, 2013).

Accumulating evidence suggests an interaction between glutamate and the catecholamine system, indicating that the glutamatergic system may be involved in ADHD pathogenesis (Kotecha et al., 2002). An international ADHD genetic study found that the "glutamate gene" panel is associated with severity of hyperactivity/impulsivity (Naaijen et al., 2017). Another study reported that dysfunctional glutamatergic neurotransmission is responsible for ADHD symptoms in the anterior cingulate cortex of adult subjects (Bauer et al., 2018). In addition, the function and expression of ionic glutamate receptors, such as α-amino-3-hydroxy-5-methyl-4-isoxazolepropionic acid receptors (AMPARs), are disrupted in the prefrontal cortices (Cheng et al., 2017) and hippocampi (Medin et al., 2019) of spontaneously hypertensive rats in well-established ADHD models. Mice lacking AMPAR subunits exhibit ADHD-like behaviors, such as hyperlocomotion (Aitta-Aho et al., 2019) and spatial working memory impairment (Reisel et al., 2002). Positive allosteric modulators of AMPARs inhibit locomotor hyperactivity in animal ADHD models and improve symptoms in adult subjects with ADHD (Adler et al., 2012). These results imply that AMPARs may be key contributors to ADHD phenotypes.

To further explore the pathophysiological mechanisms of AMPARs in ADHD, we focused on the transmembrane AMPAR regulatory protein γ-8 (TARP γ-8, also known as calcium voltage-gated channel auxiliary subunit gamma 8 (CACNG8)), which is markedly enriched in the hippocampus and modestly expressed in the cerebral cortex (Tomita et al., 2003). TARP γ-8 is a critical protein for basal AMPAR expression, trafficking, localization during synaptic development, and plasticity (Fukaya et al., 2006; Rouach et al., 2005). Recent studies have suggested that TARP γ-8 deficiency is closely associated with hyperactive behaviors. For instance, adult TARP γ-8 knockout (KO) mice are mildly hyperactive in the locomotor arena (Gleason et al., 2015) and exhibit impulsivity and aggression (Peng et al., 2021). Moreover, selective antagonists of TARP γ-8-associated AMPARs in rats produce a mild increase in locomotion, working memory impairment, and modest learning deficits (Witkin et al., 2017).

In the present study, we provide strong evidence that TARP γ-8 deficiency is closely associated with the development of ADHD. The behavioral results showed that adolescent TARP γ-8 KO mice exhibited MPH-sensitive ADHD-like phenotypes. The TARP γ-8 KO mice also displayed ADHD-like changes in the synaptosomal proteomes in the prefrontal cortex and hippocampus, which were rescued by MPH. Phenome-wide association study in humans further clarified the significant association between *CACNG8* and ADHD. Therefore, our results suggest that TARP γ-8 is involved in the pathological development of ADHD.

MATERIALS AND METHODS

Mice and reagents

All animal studies were performed in accordance with the regulations of the ARRIVE guidelines for reporting experiments (NC3Rs Reporting Guidelines Working Group, 2010). The study was approved by the Ethics Committee of Hebei Medical University (Approval No.: IACUC-hebmu-2019001, Shijiazhuang, China). The TARP γ-8 KO mouse line was backcrossed to C57BL/6J mice a minimum of eight times before use in this study. Both homozygous TARP γ-8 KO mice and their wild-type (WT) littermates were obtained from cross-bred heterozygous mice. Six mice of the same genotype were housed in one cage. All mice were maintained under constant temperature (22±0.5 °C) and humidity (50%±5%), using a 12 h light/12 h dark cycle (lights on at 1900h). Food and water were provided *ad libitum*. Four- to eight-week-old male mice (weight 13.2–20.5 g) were used in all experiments. For the pharmacological rescue experiment, MPH (Sigma Aldrich, USA) was freshly prepared with saline each time. TARP γ-8 KO and WT mice were injected intraperitoneally with saline (10 mL/kg) or MPH (2 mg/kg) 30 min before the testing phase (Li et al., 2017; Won et al., 2011), respectively.

Behavioral tests

Open field test: An open field test was carried out as

described previously (Seibenhener & Wooten, 2015), with minor modifications. The apparatus consisted of four plastic chambers, each measuring 45 cm×45 cm×45 cm, with the center zone line located 10 cm from the edge. The mice were gently placed in the center of the arena at the beginning of the session. Spontaneous locomotion was recording for 30 min using SMART Video Tracking software (Panlab, Spain) (Li et al., 2017).

Elevated plus maze (EPM): The plus-maze consisted of two open arms (29 cm×5 cm) and two enclosed arms (29 cm×5 cm×15 cm) located opposite one another, with a central platform (5 cm×5 cm) positioned at the junction of the arms. The entire plus-maze was 50 cm above the floor. At the beginning of the test session, each mouse was placed in the center of the maze facing one of the open arms. Distance in the arm, number of entries, and time spent in the arm were recorded for 5 min using SMART Video Tracking software (Panlab, Spain).

Cliff avoidance reaction (CAR): The CAR paradigm is used for assessing ADHD-like impulsive behavior in rodents (Matsuoka et al., 2005). We used an inverted glass beaker (11 cm diameter, 15 cm height; more than twice the body length of the animal) placed in the center of the open field apparatus (45 cm×45 cm×45 cm). Mice were gently placed on the platform and observed for 10 min. Latency to the first jump and number of jumping events were recorded. A mouse was judged to have an intact CAR if it did not jump off the platform during the 10 min test. We calculated a percentage index for each group (Chen et al., 2015):

$$\text{CAR\%}=\text{Number of intact CAR mice}/\text{Total number of tested mice}\times 100\% \quad (1)$$

Object recognition task: An object recognition task was performed using the open field apparatus (45 cm×45 cm×45 cm). Each mouse was allowed to explore the apparatus for 5 min to habituate to the chamber before the familiarization phase. The next day, two identical objects (A1 and A2) were placed in the chamber and mice were allowed to freely explore for 5 min to familiarize themselves with the objects, then returned to their home cages for a 1 h intertrial interval. During the test phase, one of the two identical objects (A1) was replaced with a novel object (B), and mice were allowed to explore freely for 5 min. Time spent exploring each object was recorded using SMART Video Tracking software (Panlab, Spain). All familiar (A) and novel objects (B) were made of the same wooden material with a similar smell, color, and size but differences in shape. We defined object exploration as each instance in which the mouse's nose touched the object or was oriented toward and came within 2 cm of the object. Novel object preference was determined as follows:

$$\text{Discrimination ratio (\%)}=(B-A2)/(B+A2)\times 100\% \quad (2)$$

Saline or MPH was injected intraperitoneally 30 min before the familiarization phase for pharmacological rescue experiments.

Contextual fear conditioning: Contextual fear conditioning was performed as per previous study (Xu et al., 2015), with some modifications. After three consecutive days of handling, the mice were placed in the training chamber on the day of the experiment and allowed to habituate for 120 s without any stimulation. After this, the mice received a footshock (0.7 mA, 2 s) through the stainless-steel grid floor (Panlab, Spain) followed by a 58 s interval. The 2 s/58 s procedure was repeated three times, and the mice were returned to their home cages after the final 58 s period. The chamber was cleaned with 75% alcohol. Short-term memory (STM) and long-term memory (LTM) were tested 1 and 24 h after training, respectively. The mice were placed in the same chamber for 5 min without footshock. Memory was assessed by measuring freezing behavior, defined as the complete lack of movement except for respiration and heartbeat associated with a crouching posture. Freezing time was analyzed using the PACKWIN animal behavior analysis system (Panlab, Spain), and memory score was determined as follows:

$$\text{Freezing time (\%)}=(\text{Time spent freezing})/(\text{Total time})\times 100\% \quad (3)$$

For the pharmacological rescue experiment, saline or MPH was injected 30 min before the training phase.

Phenome-wide association study on CACNG8 and ADHD

CACNG7, *CACNG8*, and *CACNG6* are located closely together on chromosome 19. Here, we conducted a large-scale phenome-wide association study of the entire *CACNG7-8-6* gene cluster and neuropsychiatric disorders to identify the phenotypes associated with *CACNG7-8-6* gene variants. We analyzed a total of 90 302 subjects from 44 independent cohorts encompassing 14 different neuropsychiatric disorders, including ADHD, schizophrenia, major depression, bipolar disorder, autism, alcoholism, nicotine dependence, Alzheimer's disease, antisocial personality disorder, Parkinson's disease, multiple sclerosis, amyotrophic lateral sclerosis, stroke, and ischemic stroke. All subjects were genotyped using microarray technology. Untyped single-nucleotide polymorphisms (SNPs) across the entire *CACNG7-8-6* gene cluster were imputed in all cohorts. SNP-disease associations were analyzed within each cohort, and the regulatory effects of disease-risk alleles on *CACNG8* mRNA expression in the brain and cortical surface area (SA) and thickness (TH) were tested in a sample of 36 936 subjects. Additional details are provided in the Supplementary Materials.

Synaptosomal proteomics

Tissue collection and synaptosome enrichment: The WT, TARP γ-8 KO, and TARP γ-8 KO (MPH) groups received intraperitoneal injections of saline or MPH for three consecutive days, respectively. Mice (n=9 per group) were anesthetized using isoflurane after the last MPH injection, and the prefrontal cortex and hippocampus were isolated, frozen in liquid nitrogen, and stored at −80 °C. Following our previous study (Kong et al., 2018), nine prefrontal cortex or hippocampus samples from each group were randomly pooled into three parts. The pooled tissues were homogenized in 1 mL of 0.32 mol/L sucrose buffer (0.32 mol/L sucrose, 5.0 mmol/L Tris-HCl, 1.0 mmol/L EDTA, pH 7.4) and 10 μL of EDTA-free protease inhibitor cocktail (Bimake, USA) using a prechilled auto-homogenizer (Jinxin Tissuelyser-24, China) for two cycles (60 Hz, 30 s). Nuclei and unhomogenized cell debris were removed by centrifugation at 1 000 ×g for 10 min at 4 °C, and the pellet containing crude synaptosome extracts

was obtained by centrifugation at 17 000 ×*g* for 10 min at 4 °C. The pellet was resuspended in 0.32 mol/L sucrose buffer and loaded onto a discontinuous top down gradient of 3%, 10%, and 23% Percoll (v/v) (Solarbio, China), then centrifuged at 31 400 ×*g* for 5 min at 4 °C using an Optima XPN-100 Superspeed Centrifuge (Beckman Coulter, USA) with a TYPE 45Ti rotor head. The interfaces between 10% and 23% were collected and subjected to dilution four times with 0.32 mol/L sucrose buffer. The synaptosome fraction was then washed twice to remove Percoll and collected by centrifugation at 17 000 ×*g* for 15 min at 4 °C. Final synaptosomal pellets were stored at −80 °C before use.

Proteomic sample preparation and tandem mass tag (TMT) labeling: Each synaptosomal sample was lysed in 8 mol/L urea on ice for 30 min (8 mol/L urea, 50 mmol/L Tris-HCl, pH 8.0). Protein concentration was determined using a BCA kit (Tiangen Biotech, China). The extracted protein (80 μg) was reduced with 100 mmol/L dithiothreitol (DTT) at 37 °C for 1 h, then alkylated with 500 mmol/L iodoacetamide (IAM) at 25 °C for 45 min. Both steps were conducted in darkness with consistent oscillation at 600 r/min in a Thermo-Shaker (AOSHENG, China), followed by the addition of six volumes of ice-cold acetone and incubation at −20 °C overnight for protein precipitation. The proteins were pelleted and air-dried to remove residual acetone. For the digestion step, the protein pellets were resuspended with 100 μL of 50 mmol/L TEAB (pH 8.5) and digested with Lys-C enzyme (Promega, China) (enzyme:substrate=1:150, w/w) at 37 °C for 3 h. Subsequently, digestion was continued by adding sequencing-grade modified trypsin (Promega, China) (enzyme: substrate=1:100, w/w) at 37 °C overnight. Finally, digestion was terminated by the addition of 10 μL of 2% formic acid (FA) to a 0.2% final concentration. The solution was then vortex for 3 min and centrifuged at 15 000 ×*g* for 10 min at 4 °C, with the resulting supernatant desalted on a MonoSpin® C18 spin column (GL Science, Japan). The eluted peptides were dried and stored at −20 °C.

For TMT labeling, consistent with our previous research (Kong et al., 2018), nine prefrontal cortex samples were individually labeled with nine labeling reagents from the TMT 10 plex™ isobaric label reagent set (Thermo Scientific, USA), with the same procedure performed for the nine hippocampus samples. Each sample consisting of 30 μg of protein in 50 μL of TEAB buffer (pH 8.5) containing 60% acetonitrile (ACN) was mixed with 30 μL of the corresponding TMT reagent for 2 h at 26 °C. The reactions were then quenched by adding 5% hydroxylamine for a further 30 min incubation at room temperature. Nine samples were mixed in equal proportions and desalted using a Sep-Pak tC18 1-cc Vac Cartridge (Waters, USA). The eluted peptides were then dried in a centrifugal evaporator. The mixed TMT-labeled peptides were redissolved in 110 μL of mobile phase A (2% ACN, pH 10.0) and separated using a Waters ACQUITY UPLC® BEH C18 column (1.7 μm×2.1 mm×100 mm) (Waters, USA) in a Dionex UltiMate 3000 RSLC system (Thermo Scientific, USA) with a 60 min gradient starting from 4% to 80% mobile phase B (98% CAN, pH 10.0) at a flow rate of 0.2 mL/min. Twelve fractions were collected over the gradient at 1 min intervals and were dried to completion. The peptide samples were resuspended in 0.1% FA for subsequent nano-scale liquid chromatography tandem mass spectrometry (nLC-MS/MS).

nLC-MS/MS analysis: Following our previous study (Kong et al., 2018), the TMT-labeled peptides were determined using the Thermo Easy nLC 1000 UPLC system (Thermo Fisher Scientific, USA) coupled to an Orbitrap Fusion mass spectrometer with a NanoFlex source (Thermo Fisher Scientific, USA). The peptide mixture was separated using a homemade fused silica capillary column (75 μm×200 mm) packed with C18 resin (3 μm, Aqua C18, Phenomenex, USA). The online separation gradient consisted of buffer A (0.1% FA) and buffer B (ACN, 0.1% FA) delivered at a flow rate of 300 nL/min for 90 min. The gradient was as follows: 4%–8% B from 0 to 2 min, 8%–25% B from 2 to 67 min, 25%–60% B from 67 to 80 min, 60%–95% B from 80 to 81 min, and 95% B from 81 to 90 min. Data-dependent acquisition (DDA) was applied using the Orbitrap Fusion mass spectrometer (Thermo Scientific, USA). For MS, a full scan was acquired in the 350–1 950 m/z range at a resolution of 60 000. A quadrupole with a transmission window of 1 m/z was used to isolate ion filtering for MS/MS events. Higher-energy collisional dissociation (HCD) fragmentation was performed with 38% normalized collision energy, followed by analysis of the fragment ions in the Orbitrap Fusion mass spectrometer with a resolution of 60 000. The duty cycle was fixed at 3 s. The automatic gain control (AGC) settings were $2\times e^5$ and $1\times e^5$ ions and maximal ion injection times of 60 and 100 ms were set for full and MS2 scans, respectively.

Protein identification and bioinformatic analysis: Proteome Discoverer v2.1 (Thermo Fisher Scientific, USA) was used to analyze raw instrument files, which were combined in 12 fraction files and searched against the *Mus musculus* proteome database (updated in August 2021; 55 336 proteins) using the SEQUEST HT search engine. The search parameters were set to: trypsin cleavage allowing up to two missed cleavages; precursor mass tolerance of 10 ppm; fragment ion mass tolerance of 0.02 Da; false discovery rate (FDR) cutoff of 1% at the peptide and protein levels. Matching protein entries requires at least one unique peptide for identification. Thus, before downstream analysis, bait proteins and contaminants were removed from all datasets. Abundances per channel were normalized and scaled by total abundance of identified peptides. Partial least squares discriminant analysis (PLS-DA) was performed to investigate differences in proteomic characteristics. Differentially expressed proteins (DEPs) were filtered based on 1.2-fold-change (≥1.2 or ≤0.8) and $P<0.05$ using volcano plot analysis. Subsequently, DEPs were loaded onto the DAVID online platform (https://david.ncifcrf.gov) for functional enrichment analysis using Kyoto Encyclopedia of Genes and Genomes (KEGG) and Gene Ontology (GO). The online STRING database (http://string-db.org/) was used to analyze protein-protein interactions of the DEPs induced by TARP γ-8 and MPH, and Cytoscape v3.8.2 and its plugin BiNGO v3.0.5 (National Resource for Network Biology, USA) were used to visualize the network and detect functional clusters, respectively.

Electrophysiological recordings of acute brain slices

Male mice (aged 6 and 8 weeks) were anesthetized and decapitated. Coronal brain slices (300 μm) were prepared using a model 7000 smz vibratome (Campden Instruments, USA). Dissected brain tissue samples were placed in an ice-cold slice solution (pH 7.4) containing (in mmol/L): 92 NMDG, 1.2 NaH_2PO_4•H_2O, 30 $NaHCO_3$, 20 HEPES, 25 glucose, 5 sodium ascorbate, 2 thiourea, 3 sodium pyruvate, 2.5 KCl, 10 $MgSO_4$, and 0.5 $CaCl_2$. The slices were allowed to recover at 32 °C in aerated artificial cerebrospinal fluid (ACSF; pH 7.4) containing (in mmol/L): 92 NaCl, 1.2 NaH_2PO_4•H_2O, 30 $NaHCO_3$, 20 HEPES, 25 glucose, 5 sodium ascorbate, 2 thiourea, 3 sodium pyruvate, 2.5 KCl, 1 $MgSO_4$, 2 $CaCl_2$, and 1.2 N-acetyl-L-cysteine. After 30 min, the slices were stored at room temperature, then transferred to a submersion recording chamber and perfused with aerated ACSF (pH 7.4) containing (in mmol/L): 125 NaCl, 1.25 NaH_2PO_4•H_2O, 26 $NaHCO_3$, 11 glucose, 2.5 KCl, 1 $MgSO_4$, and 2.4 $CaCl_2$. All solutions were constantly oxygenated with 95% O_2/5% CO_2. Pyramidal neuronal activity in the hippocampal CA1 was recorded using voltage-clamp mode with 3 kHz filtration and 20 kHz digitization as reported previously (Yu et al., 2020). Patch electrodes with a resistance of 3–6 MΩ were pulled using a P-97 micropipette puller (Sutter Instrument, USA). The internal solution contained (in mmol/L): 117 Cs- methanesulfonate, 20 HEPES, 2.8 NaCl, 4 MgATP, 0.3 Na_3GTP, 0.4 EGTA, and 5 QX-314 (pH adjusted to 7.3–7.4 with CsOH). To record evoked excitatory postsynaptic currents (eEPSCs), we placed the bipolar metal electrode (CBBRC75, FHC, USA) in the stratum radiatum at a distance of 100–200 μm from the recorded pyramidal neurons. Stimuli were generated using an ISO-Flex stimulator (AMPI, Israel) at 0.1 Hz for 0.1 ms. The holding potential was set to −70 mV. AMPAR-mediated eEPSCs were recorded in ACSF containing 0.1 mmol/L PTX, 10 μmol/L bicuculline, and 50 μmol/L amino-5-phosphonopentanoic acid.

Statistical analysis

All data are represented as mean±standard error of the mean (*SEM*), unless otherwise specified. Statistical analysis was performed using GraphPad Prism v8.0.2 (GraphPad, USA). For comparisons of animal behavior, data normality was analyzed using the Shapiro-Wilk test. Normally distributed data were analyzed using unpaired student's *t*-test or two-way analysis of variance (ANOVA) followed by Bonferroni-corrected *post hoc* multiple comparisons. Non-normally distributed data were analyzed by nonparametric Mann-Whitney or Kruskal-Wallis tests followed by Dunn's multiple comparison tests. CAR data (%) were compared using the Log-Rank (Mantel-Cox) test. For electrophysiological recordings of acute brain slices, paired student's *t*-test was used to compare the effects of MPH on the amplitude of AMPAR eEPSCs. $P<0.05$ was set as the threshold for significance (*: $P<0.05$; **: $P<0.01$; ***: $P<0.001$).

RESULTS

Adolescent TARP γ-8 KO mice exhibited hyperactivity and anxiety-like behaviors

Adult TARP γ-8 KO mice exhibit obvious hyperactivity in novel environments (Gleason et al., 2015; Peng et al., 2021). Here, to test whether TARP γ-8 deficiency is associated with the ADHD patient-like phenotype in adolescents, we evaluated locomotor activity in TARP γ-8 KO mice aged 4–8 weeks. Compared to WT mice, the adolescent TARP γ-8 KO mice exhibited significantly higher levels of spontaneous locomotor activity in the open field test (Figure 1A–C), including total distance (Figure 1B) and distance traveled per 5 min during the 30 min test (Figure 1C), suggesting that TARP γ-8 deficiency can lead to ADHD-like hyperactivity in adolescent mice. The adolescent TARP γ-8 KO mice also showed more activity traces in the peripheral area (Figure 1A) with less time spent in the central area of the open field (Figure 1D), indicating mild anxiety.

To investigate the anxiety-like phenotype, we examined behavioral anxiety in these mice using the classic EPM test. Compared to WT mice, the adolescent TARP γ-8 KO mice moved much farther in total distance in the EPM (Figure 1F). Although open arm movement distance was similar between the KO and WT mice, closed arm movement distance was significantly higher in KO mice than in WT mice (Figure 1E, F). No differences were observed between the two groups regarding number of entries into the arm or time spent in the closed arm (Figure 1G, H); however, adolescent TARP γ-8 KO mice spent significantly less time in the open arm compared with WT mice (Figure 1H). These results confirmed the mild anxiety-like behavior observed in adolescent TARP γ-8 KO mice.

Adolescent TARP γ-8 KO mice showed impulsivity and cognitive and memory impairment

As impulsivity is a diagnostic symptom of ADHD, we performed the CAR test to evaluate impulsivity (Matsuoka et al., 2005) in adolescent TARP γ-8 KO mice. Results showed that the latency to jump off the platform was much shorter in TARP γ-8 KO mice than in WT mice (Figure 1I). During the test period (10 min), TARP γ-8 KO mice jumped more frequently than WT mice (Figure 1J). Moreover, all TARP γ-8 KO mice jumped, whereas only 50% of WT mice jumped from a height (Figure 1K). These results suggest that loss of TARP γ-8 may lead to impulsivity.

Individuals with ADHD exhibit cognitive deficits such as impaired memory (Won et al., 2011). Thus, we evaluated cognitive and memory functions in adolescent TARP γ-8 KO mice. The object recognition test was used to assess cognitive memory, which is mainly associated with the prefrontal cortex (Barker et al., 2007; Cheng et al., 2017). Although adolescent TARP γ-8 KO mice spent more time exploring the object (Figure 1L), their discrimination ratio (%) was significantly lower than that of WT mice (Figure 1M), suggesting that the TARP γ-8 KO mice exhibited recognition memory impairment with no preference for the novel object.

Previous studies have reported that ADHD animal models show reduced contextual fear conditioning (Calzavara et al., 2009), which is also a classic paradigm for studying hippocampus-dependent memory processes (Xu et al., 2015). We evaluated contextual fear memory in TARP γ-8 KO mice. Freezing duration, defined as complete immobility of the animal in the absence of vibrissae movements and sniffing,

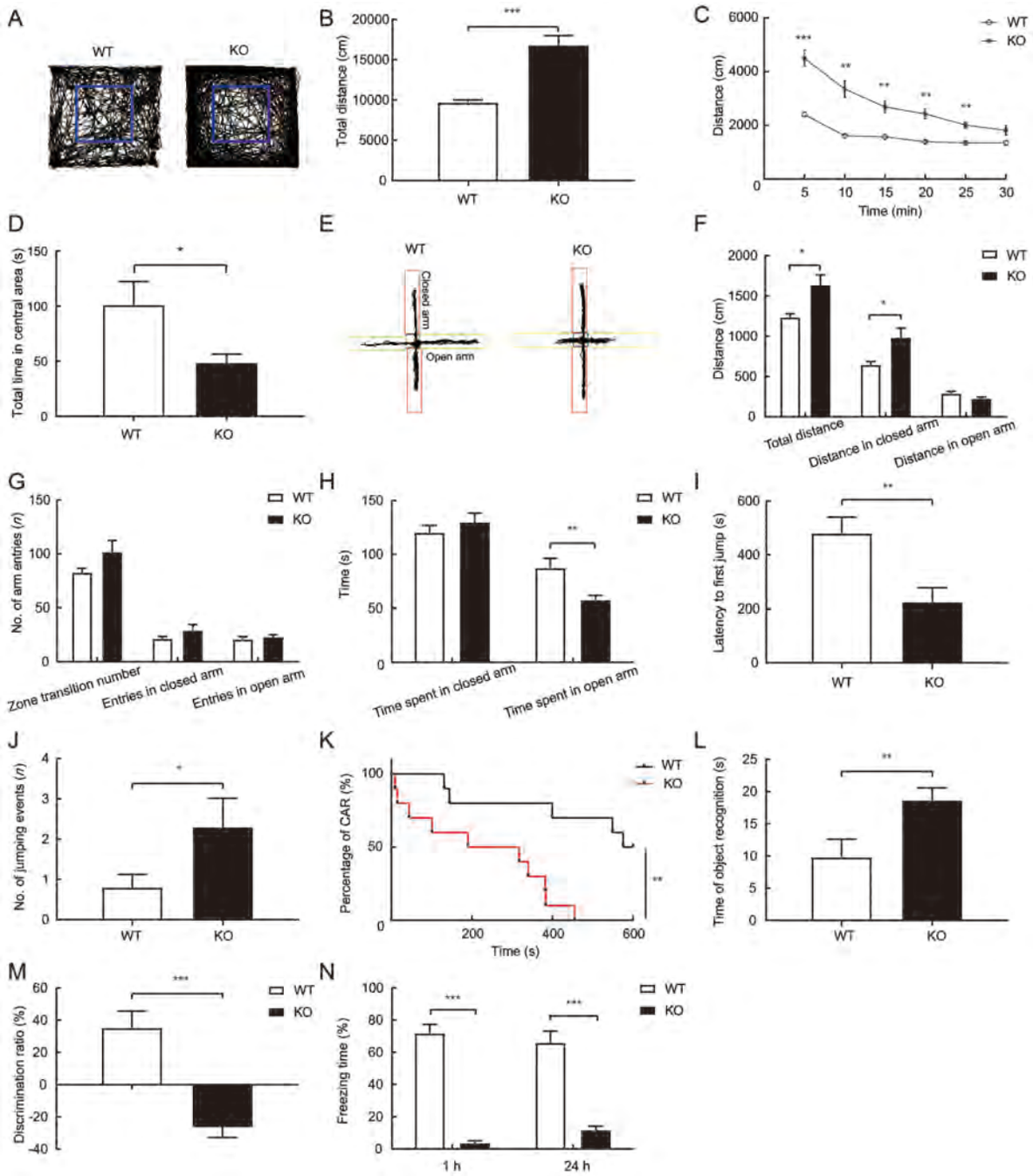

Figure 1 ADHD-like behavior in adolescent TARP γ-8 KO mice

A–D: Open field test. A: Representative activity traces in open field. Inside of blue square represents central area, outside represents peripheral area. B: Total distance traveled during 30 min. C: Distance traveled every 5 min. D: Total time spent in central area during 30 min. E–H: Elevated plus-maze (EPM). E: Video-tracking trajectory in EPM, red rectangle represents closed arm, green rectangle represents open arm. F: Distance traveled in EPM during 5 min. G: Number of arm entries. H: Time spent in closed or open arms. I–K: Cliff avoidance reaction test (CAR). I: Time from initial placement on platform to first jump in 10 min. J: Number of jumping events in 10 min. K: Percentage of mice with intact CAR. L, M: Novel object recognition test. L: Total time exploring novel and familiar objects in the testing session. M: Discrimination ratio in testing session. N: Contextual fear conditioning. Short-term memory (STM) and long-term memory (LTM) were assessed by measuring freezing behavior 1 and 24 h after training, respectively. All data are presented as mean±*SEM*, n=10 mice per group. Unpaired student's t-test was used in B, F, G, H, M, and N (24 h). Two-way repeated measures ANOVA was used in C ($F_{\text{strains}(1,\ 18)}$=32.84, P<0.0001; $F_{\text{time}(2.4,\ 44)}$=97.9, P<0.0001; $F_{\text{interaction}(5,\ 90)}$=20.18, P<0.0001), followed by Bonferroni's *post hoc* test (5 min WT vs. KO: P<0.001; 10–25 min WT vs. KO: P<0.01). Mann-Whitney test was used in D, I, J, L, and N (1 h). Comparison of CAR% between WT and KO mice using Log-Rank (Mantel-Cox) test in K. *: P<0.05; **: P<0.01; ***: P<0.001.

was quantified for 5 min. STM and LTM tests were performed 1 and 24 h after the training sessions, respectively. Results showed that freezing times (%) in the STM and LTM tests were significantly shorter in adolescent TARP γ-8 KO mice than in WT mice (Figure 1N), suggesting that TARP γ-8 deficiency is associated with memory deficits.

Taken together, these data indicate that adolescent TARP γ-8 KO mice exhibit typical characteristics of ADHD, including hyperactivity, anxiety, impulsivity, cognitive impairment, and memory deficits.

Phenome-wide association analysis showed significant association between *CACNG8* and ADHD

Given the suggested association between TARP γ-8 and ADHD, we performed phenome-wide association analysis in humans. A total of 491 SNPs within the *CACNG7-8-6* gene cluster were examined, including 126 within *CACNG7*, 137 within *CACNG8*, and 228 within *CACNG6*. After Bonferroni's correction ($\alpha=2.3\times10^{-6}$), *CACNG7-8-6* variants were only significantly associated with ADHD in the "IMAGE" cohort ($P=2.7\times10^{-9}$ for rs11084307 at *CACNG8*; Supplementary Table S1) and with major depression in the "GenTransTwinsMD" cohort ($P=9.8\times10^{-8}$ for rs12610534 at *CACNG6*; Supplementary Table S1).

A total of 18 SNPs were nominally significantly associated with ADHD in the "IMAGE" cohort ($P<0.05$), with the most significant associations found for rs11084307 ($P=2.7\times10^{-9}$) and rs10420331 ($P=0.014$; Table 1), a SNP closely linked to rs11084307. To date, only two *CACNG8* SNPs have been reported to be associated with neuropsychiatric disorders (Guan et al., 2016). Here, we found that the rs11084307-rs10420331 haplotypes were significantly associated with schizophrenia ($P=1.4\times10^{-6}$; Table 1). Associations between SNPs and ADHD were replicable in the "ABCD-twin" cohort in the same effect direction ($P=0.050$ and 0.040, respectively); i.e., allele T of rs11084307 and allele G of rs10420331 increased the risk of ADHD in both cohorts (Table 1). Both alleles also increased the risk of Parkinson's disease, multiple sclerosis, and schizophrenia (in one cohort), but decreased the risk of major depression. Allele T of rs11084307 also decreased the risk of schizophrenia in an Ashkenazi Jewish cohort (Table 1). These results indicated that the associations between *CACNG8* variants and ADHD were replicable. In addition, the ADHD-risk alleles, i.e., allele T of rs11084307 and allele G of rs10420331, significantly increased cortical surface areas (SA) of the brain ($P=0.011$ and 0.047, respectively) and insula ($P=0.049$ for T of rs11084307) and decreased cortical thickness (TH) of the pars triangularis ($P=0.020$ and 0.001, respectively; Table 2). These results suggest that the ADHD-risk variants at *CACNG8*, i.e., rs11084307 and rs10420331, are biologically functional.

Proteomic identification of synaptosomes of prefrontal cortex and hippocampus

Synapses are essential structures for transmitting information in the brain. Synaptic dysfunction in the central nervous system can be either the cause or consequence of central neurological disorders. Similar to many other neurological disorders, ADHD likely results from synaptic dysfunction. To explore the synaptic mechanisms underlying ADHD-like phenotypes induced by TARP γ-8 deletion, we explored molecular alterations in the synaptosomes of the prefrontal cortex (Shaw et al., 2007) and hippocampus (Posner et al., 2014), which not only encode cognition and memory but also preferentially express TARP γ-8 (Tomita et al., 2003). A total of 4 192 and 4 170 master proteins were identified in the cortical and hippocampal synaptosomes, respectively, of which 3 431 proteins overlapped in the two brain regions (Figure 2A).

Identification of synaptosome DEPs induced by TARP γ-8 KO

To investigate differences in the proteomic characteristics of synaptosomes between TARP γ-8 KO and WT mice, PLS-DA was performed. All 4 192 proteins from the cortical

Table 1 Replicable associations between *CACNG8* variants and neuropsychiatric disorders

			IMAGE	ABCD-twin	Ing_coriell	GSK_MS	PMID: 27102562	SCZ		AJ_SZ		GenomTrans
			European Family-based	European Family-based	European Case-control	European Case-control	Chinese[#] Case-control	Chinese Case-control		European Case-control		European Family-based
	Genomic		Risk alleles and *P*-values							Risk alleles and *P*-values		
SNP	position		ADHD	ADHD	Parkinson	MS	Schizophrenia	Schizophrenia		Schizophrenia		MD
rs11084307	59172962	T	2.7×10^{-9}	0.050	0.027	0.003	1.4×10^{-6}	0.350	C*	0.039	C	0.586
rs10420331	59160880	G	0.014	0.040	0.046	0.026	1.4×10^{-6}	0.026	G	0.031	A	0.019

1st header row: dataset names correspond to Supplementary Table S1; 2nd header row: ethnicity; 3rd header row: study design; 5th header row: diagnosis. #: *P*-values correspond to rs11084307–rs10420331 haplotypes (PMID: 27102562). *: Risk allele is only exception in effect direction.

Table 2 Regulatory effects of ADHD-risk alleles on cortical SA and TH

	Genomic	Effective allele and *P*-value			Effective allele and *P*-value	
SNP	position	Allele	Full SA	Insular SA	Allele	Pars triangularis TH
rs11084307	59172962	T	0.011	0.049	C	0.020
rs10420331	59160880	G	0.047	0.135	A	0.001

SA, cortical surface area; TH, cortical thickness; Full SA, surface area of whole brain.

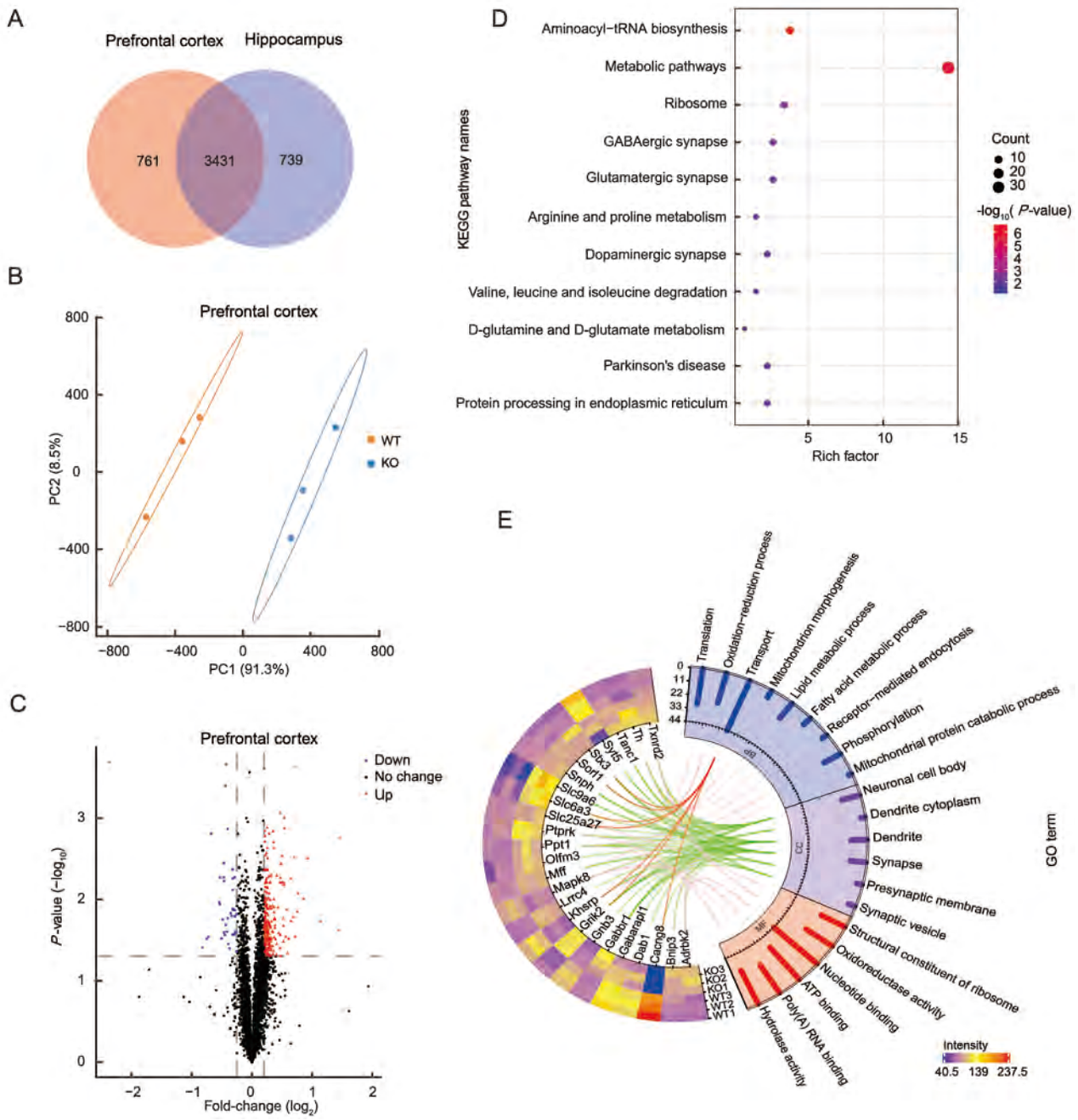

Figure 2 Proteomic analysis of identified proteins and DEPs induced by TARP γ-8 KO in prefrontal cortical synaptosomes

A: Venn diagram of identified proteins. In total, 4 192 proteins were identified in prefrontal cortical synaptosome (red circle), 4 170 proteins were identified in hippocampal synaptosome (blue circle), and 3 431 proteins were co-identified. B: PLS-DA of identified proteins from prefrontal cortical synaptosome. C: Volcano plots of identified proteins from prefrontal cortex. Red points represent fold-change≥1.2 and P<0.05, blue points represent fold-change≤0.8 and P<0.05. D: Bubble chart of enriched KEGG pathways in DEPs induced by TARP γ-8 in prefrontal cortical synaptosome. X-axis represents Rich factor, with larger values indicating greater proportion of DEPs annotated to pathway. Y-axis represents KEGG pathway annotation entries. Dot size represents count of DEPs annotated to pathway. Dot color represent statistical significance of enriched KEGG pathway ($-\log_{10}P$-value), blue is lowest and red is highest significance. E: Heat map of synapse-related DEPs based on GO enrichment analysis. Color scale of heat map indicates abundance of DEPs, blue is lowest and red is highest. GO enrichment analysis of biological processes (BP), cellular components (CC), and molecular functions (MF) of synapse-related DEPs. Bar plot indicates count of DEPs. For each category, P<0.05 was defined as significant. GO terms are sorted clockwise according to significance.

synaptosomes were analyzed by PLS-DA and a score plot was generated (Figure 2B). The score plot and ellipses corresponding to 95% confidence intervals showed excellent separation between the TARP γ-8 KO and WT cortical synaptosomes. Principal component 1 accounted for 91.3% of total variance (Figure 2B). Similarly, all 4 170 proteins from the hippocampal synaptosomes were analyzed by PLS-DA, revealing a clear separation between the TARP γ-8 KO and WT groups (Figure 3A). Principal component 1 accounted for 94.4% of total variance (Figure 3A). These results suggest that proteomic profiles are altered in the prefrontal cortex and hippocampus by the deletion of TARP γ-8 in adolescent mice.

Fold-changes in the identified proteins were calculated as the TMT-plex reporter ion abundance ratio of any given

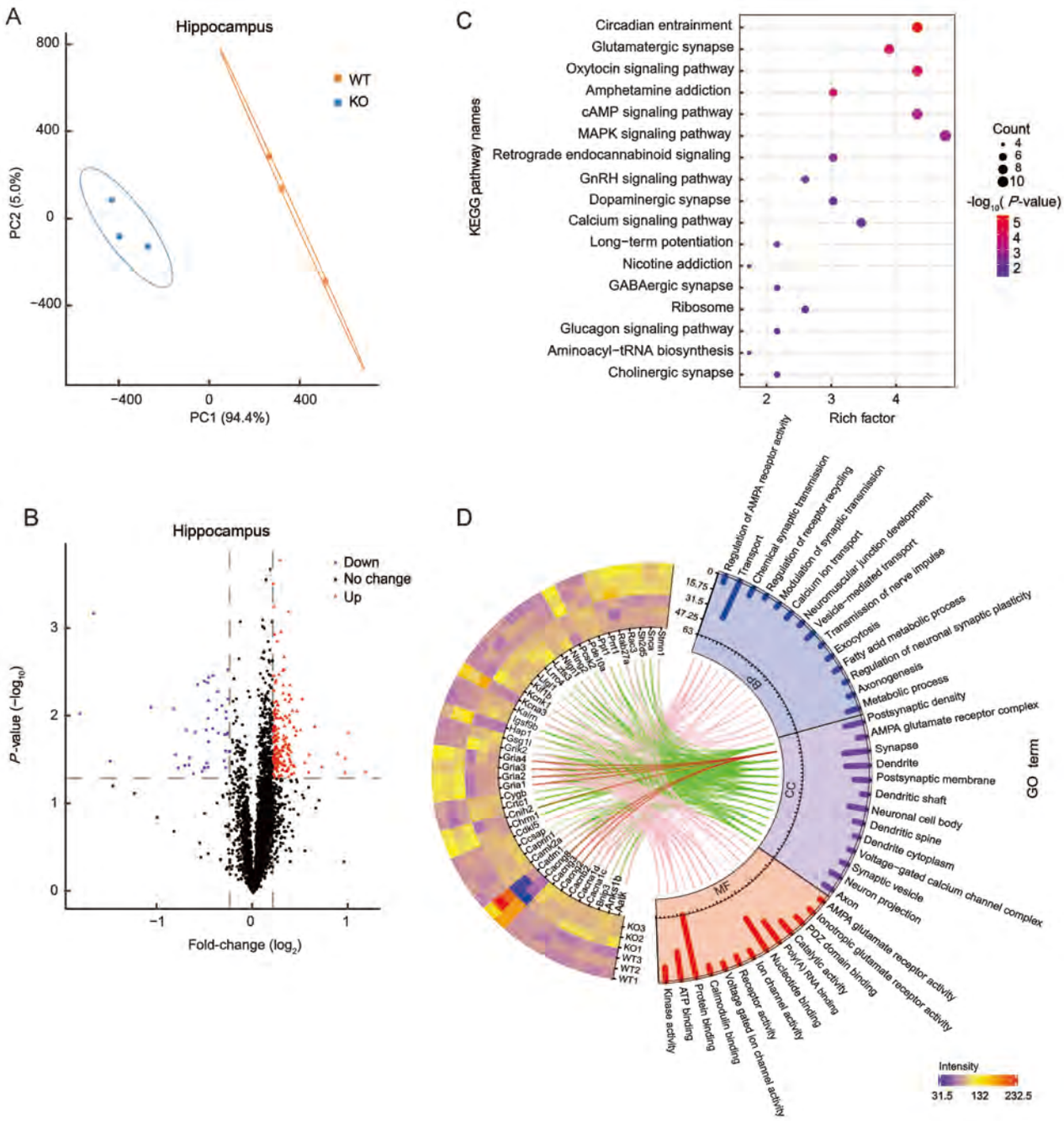

Figure 3 Proteomic analysis of identified proteins and DEPs induced by TARP γ-8 KO in hippocampal synaptosomes

A: PLS-DA of identified proteins from hippocampal synaptosomes. B: Volcano plots of identified proteins from hippocampal synaptosomes. Red points represent fold-change≥1.2 and P<0.05, blue points represent fold-change≤0.8 and P<0.05. C: Bubble chart of enriched KEGG pathways in DEPs in hippocampal synaptosomes. X-axis represents Rich factor, Y-axis represents KEGG pathway annotation entries. D: Heat map of synapse-related DEPs with GO enrichment analysis.

protein between the TARP γ-8 KO and WT groups. The DEPs were determined based on cutoff values (≥1.2 or ≤0.8 for up-regulated and down-regulated proteins, respectively, P<0.05). Volcano plots were generated, with $\log_2$ fold-changes on the X-axis and negative logarithm of P-values on the Y-axis. A total of 265 DEPs (Supplementary Table S2) were identified in the mouse cortical synaptosomes, including 224 significantly up-regulated proteins and 41 significantly down-regulated proteins (Figure 2C). For the hippocampal synaptosomes, volcano plots identified 235 DEPs (Supplementary Table S3), including 191 significantly up-regulated proteins and 44 significantly down-regulated proteins (Figure 3B).

KEGG pathway and GO functional analysis of DEPs from cortical and hippocampal synaptosomes

Based on the 265 DEPs in the cortical synaptosomes, KEGG pathway analysis was performed to characterize the biological regulation of abnormal behavior. Results revealed a total of 11 pathways (Figure 2D), with the top three pathways, i.e., aminoacyl-tRNA biosynthesis (P=2.66×10^{-7}), metabolic (P=3.56×10^{-6}), and ribosomal (P=8.89×10^{-4}), significantly enriched (P<0.001). In addition to the top three pathways associated with biological regulation, the GABAergic (P=1.27×10^{-3}), glutamatergic (P=5.21×10^{-3}), and dopaminergic synapses (P=3.86×10^{-2}), which play distinct roles in neuronal connectivity in cognitive function, were significantly enriched (P<0.05). These findings are consistent with recent research in ADHD showing dopaminergic (Del Campo et al., 2011), glutamatergic (Cheng et al., 2017), and GABAergic (Solleveld et al., 2017) transmission dysfunction in the prefrontal cortex. GO annotation analysis was performed to further investigate the potential functions of cortical synaptic proteins. We filtered and visualized 25 synapse-associated proteins using a heat map (Figure 2E), including 18 up-regulated and seven down-regulated proteins. As shown in Figure 2E, cellular component analysis revealed that the 25 DEPs were mainly located in neuronal cell bodies, dendritic cytoplasm, dendrites, synapses, presynaptic membranes, and synaptic vesicles (Figure 2E, green lines). The functions of these DEPs were associated with multiple biological processes, including translation, oxidation-reduction, and transport. Seven DEPs (Cacng8, Grik2, Khsrp, Slc25a27, Slc6a3, Sorl1, and Stx3) were associated with transport function (Figure 2E, red lines). Notably, Grik2, a member of the ionotropic glutamate receptor, was identified as potentially sensitive to psychiatric disorders (Shaltiel et al., 2008). Furthermore, the dopamine transporter gene *Slc6a3* is highly correlated with ADHD and is the main target of MPH (Reith et al., 2022).

For the hippocampal synaptosomes, the 235 DEPs were subjected to KEGG pathway enrichment analysis. We identified a total of 17 enriched pathways (Figure 3C), including the circadian entrainment (P=5.26×10^{-6}), glutamatergic synapse (P=1.33×10^{-4}), oxytocin signaling (P=1.57×10^{-4}), and amphetamine addiction (P=2.43×10^{-4}) pathways, which were significantly enriched (P<0.001). Dopaminergic synapses (P=8.59×10^{-3}), calcium signaling pathways (P=9.77×10^{-3}), long-term potentiation (P=1.12×10^{-2}), nicotine addiction (P=1.56×10^{-2}), and GABAergic synapses (P=2.80×10^{-2}) were also significantly enriched (P<0.05). These findings indicate that disorders related to learning, memory, reward, and hyperactivity in hippocampal synapses are induced by TARP γ-8 deletion. Similarly, GO enrichment analysis revealed 44 synapse-associated proteins, which were filtered and visualized using a heat map (Figure 3D) and included 27 up-regulated and 17 down-regulated proteins. Cellular component analysis revealed that the AMPA glutamate receptor complex was clearly associated with Gria1–4 and AMPAR regulatory proteins (Cacng2, Cacng3, Cacng8, and Cnih2) (Figure 3D, red lines). Cacng8 was down-regulated in TARP γ-8 KO mice, as were Gria1, Gria2, Gria3, Gria4, and Cnih2. Interestingly, Cacng2 and Cacng3 expression levels were up-regulated (Figure 3D). Biological process analysis revealed chemical synaptic transmission dysfunction (associated with Gria1, Gria2, Gria4, Grik2, Cacnb2, Cacna1c, and Snca) and neuronal synaptic plasticity regulation (associated with Camk2a, Kalrn, and Snca). Molecular function analysis similarly revealed dysfunction in glutamate and ionotropic glutamate receptor activity. These findings suggest that AMPARs in hippocampal synaptosomes are dysfunctional in TARP γ-8 KO model pathology, thus playing a key role in learning and memory in the hippocampus.

MPH alleviated hyperactivity induced by TARP γ-8 KO but aggravated anxiety in adolescent TARP γ-8 KO and WT mice

Based on the above results, we found that TARP γ-8 KO altered the dopamine transporter Slc6a3, which is the primary target of MPH, the first-line treatment for ADHD (Posner et al., 2020; Thapar & Cooper, 2016). We hypothesized that MPH would normalize ADHD-like phenotypes in adolescent TARP γ-8 KO mice. Indeed, the major behavioral deficits in TARP γ-8 KO mice were rapidly restored by acute administration of a clinically relevant dose of MPH (2 mg/kg) (Li et al., 2017; Won et al., 2011).

Results showed that MPH administration significantly decreased the total distance traveled by TARP γ-8 KO mice in the open field test (Figure 4A) but did not increase time spent in the central area (Figure 4B). We also conducted the EPM anxiety test for MPH treatment. Results indicated that MPH administration significantly increased total distance traveled by WT mice compared to the saline group (Figure 4C). Although MPH also increased total travel distance in TARP γ-8 KO mice, this increase was not statistically significant (Figure 4C). Similarly, MPH increased distance (Figure 4C), number of entries (Figure 4D), and time spent in the closed arms (Figure 4E) in WT mice compared to the saline-treated mice. In addition, MPH significantly decreased time spent in the open arms in both WT and KO mice (Figure 4E). These findings suggest that MPH aggravates anxiety in adolescent TARP γ-8 KO and WT mice, consistent with the adverse drug reactions reported in the clinical use of MPH (Pozzi et al., 2019).

MPH had little effect on impulsivity but significantly improved cognition and memory in adolescent TARP γ-8 KO mice

We next examined the impact of MPH on impulsive behavior

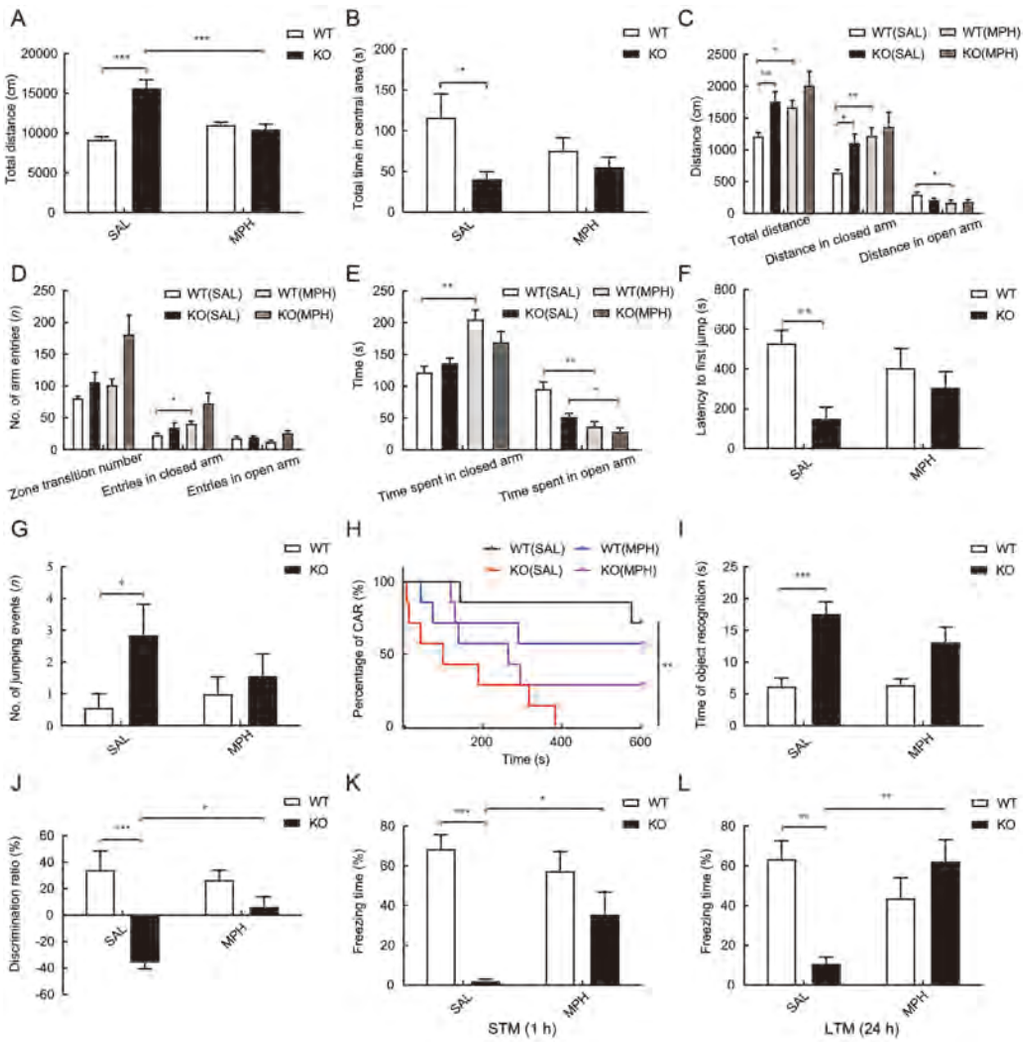

Figure 4 MPH alleviated hyperactivity and improved impaired cognitive and memory behaviors despite aggravating anxiety, but had little effect on impulsivity in adolescent TARP γ-8 KO mice

A, B: Open field test in WT and KO mice treated with saline or MPH (2 mg/kg, i.p., 30 min before testing). A: Total distance traveled in 30 min: Two-way ANOVA ($F_{strains(1, 24)}$=22.24, P<0.0001; $F_{treatment(1, 24)}$=7.179, P=0.013; $F_{interaction(1, 24)}$=31.32, P<0.0001), followed by Bonferroni's *post hoc* test (SAL+WT vs. SAL+KO: P<0.0001; SAL+KO vs. MPH+KO: P<0.0001). B: Total time spent in central area in 30 min: Two-way ANOVA ($F_{strains(1, 24)}$=7.164, P=0.013; $F_{treatment(1, 24)}$=0.547, P=0.466; $F_{interaction(1, 24)}$=2.354, P=0.138), Bonferroni's *post hoc* test (SAL+WT vs. SAL+KO: P<0.05). C–E: EPM task. C: Total distance: Kruskal-Wallis test (H_2=12.690, P=0.005), Dunn's test (SAL+WT vs. SAL+KO: P=0.007; SAL+WT vs. MPH+WT: P=0.011); distance in closed arm: Kruskal-Wallis test (H_2=11.500, P=0.009), Dunn's test (SAL+WT vs. SAL+KO: P=0.021; SAL+WT vs. MPH+WT: P=0.002); distance in open arm: Kruskal-Wallis test (H_2=7.560, P=0.056), Dunn's test (SAL+WT vs. MPH+WT: P=0.012). D: Number of arm entries. Entries in closed arm: Kruskal-Wallis test (H_2=9.653, P=0.021), Dunn's test (SAL+WT vs. MPH+WT: P=0.017). E: Time spent in closed or open arms. Time spent in closed arm: Kruskal-Wallis test (H_2=12.980, P=0.004), Dunn's test (SAL+WT vs. MPH+WT: P=0.001); Time spent in open arm: Kruskal-Wallis test (H_2=17.31, P=0.0006), Dunn's test (SAL+WT vs. MPH+WT: P=0.002; SAL+KO vs. MPH+KO: P=0.034). F–H: CAR test. F: Latency to first jump: Kruskal-Wallis test (H_2=9.172, P=0.027), Dunn's test (SAL+WT vs. SAL+KO: P=0.003). G: Number of jumping events: Kruskal-Wallis test (H_2=7.316, P=0.062), Dunn's test (SAL+WT vs. SAL+KO: P=0.010). H: Percentage of mice with intact CAR: Log-rank test (SAL+WT vs. SAL+KO: P=0.001). I, J: Novel object recognition test. I: Total time exploring novel and familiar objects in testing session: Two-way ANOVA ($F_{strains(1, 24)}$=28.760, P<0.001, $F_{treatment(1, 24)}$=1.563, P=0.223, $F_{interaction(1, 24)}$=1.929, P=0.177), Bonferroni's *post hoc* test (SAL+WT vs. SAL+KO: P=0.0004). J: Discrimination ratio in testing session. Two-way ANOVA ($F_{strains(1, 24)}$=26.260, P<0.0001, $F_{treatment(1, 24)}$=3.823, P=0.062, $F_{interaction(1, 24)}$=7.988, P=0.009), Bonferroni's *post hoc* test (SAL+WT vs. SAL+KO: P<0.0001; SAL+KO vs. MPH+KO: P=0.014). K, L: Contextual fear conditioning. K: Freezing time (%) of STM: Two-way ANOVA ($F_{strains(1, 24)}$=29.650, P<0.0001, $F_{treatment(1, 24)}$=1.938, P=0.176, $F_{interaction(1, 24)}$=7.615, P=0.010), Bonferroni's *post hoc* test (SAL+WT vs. SAL+KO: P<0.0001; SAL+KO vs. MPH+KO: P=0.043). L: Freezing time (%) of LTM: Two-way ANOVA ($F_{strains(1, 24)}$=3.763, P=0.064, $F_{treatment(1, 24)}$=3.249, P=0.084, $F_{interaction(1, 24)}$=16.310, P=0.0005), Bonferroni's *post hoc* test (SAL+WT vs. SAL+KO: P=0.001; SAL+KO vs. MPH+KO: P=0.002). All data are presented as mean±*SEM*, n=7 mice per group, *: P<0.05; **: P<0.01; ***: P<0.001.

in adolescent TARP γ-8 KO mice. As shown in Figure 4F–H, MPH did not affect jumping latency compared to the saline treatment group (Figure 4F). In addition, no significant difference was observed in the number of jumping events (Figure 4G) and percentage of intact CAR mice (CAR%) (Figure 4H) after MPH treatment in TARP γ-8 KO mice. These findings are similar to previous reports on impulsive behavior and MPH in other ADHD models (Bouchatta et al., 2018).

In the object recognition test, although there was a significant difference in the total time for object recognition between the saline-treated WT and TARP γ-8 KO groups (Figure 4I), MPH had no effect on total time for object recognition compared to the saline-treated TARP γ-8 KO mice. However, two-way ANOVA revealed a significant difference in the discrimination ratio (%) (Figure 4J), and Bonferroni's *post hoc* comparison showed significant impairment in recognition function (P<0.001) in the TARP γ-8 KO group treated with saline, which was obviously rescued after MPH treatment (P=0.014). In addition, MPH improved memory in adolescent TARP γ-8 KO mice. In the contextual fear conditioning test, STM freezing time (%) was analyzed using two-way ANOVA, and Bonferroni's *post hoc* test revealed that saline-treated TARP γ-8 KO mice showed shorter freezing times than saline-treated WT mice, which were significantly improved after MPH treatment (Figure 4K). A similar trend was also observed in LTM (Figure 4L), which was obviously impaired in saline-treated TARP γ-8 KO mice compared to saline-treated WT mice, with *post hoc* analysis revealing that MPH significantly improved LTM.

Proteomic analysis of effects of MPH on synaptic proteins

To further investigate the mechanism related to the effects of MPH on ADHD-like phenotypes, we performed proteomic analysis of synaptic proteins. PLS-DA revealed a clear separation between the TARP γ-8 KO and MPH-treated groups; principal component 1 accounted for 94.7% and 86.6% of total variance in the prefrontal cortical and hippocampal synaptosomes, respectively (Figures 5A, 7A). Based on the volcano plots, 114 DEPs were found in mouse cortical synaptosomes, including 85 up-regulated and 29 down-regulated proteins (Figure 5B). Regarding the hippocampal synaptosomes, 45 DEPs were identified, including 39 up-regulated and six down-regulated proteins (Figure 7B). These findings indicate that the proteomes of the cortical and hippocampal synaptosomes are obviously altered by short-term MPH treatment in TARP γ-8 KO mice.

Bioinformatic analysis of DEPs induced by MPH treatment in cortical synaptosomes

To explore the molecular mechanism of MPH treatment on behavioral deficits in TARP γ-8 KO model mice, we identified MPH-positive DEPs in cortical synaptosomes (i.e., DEPs down-regulated or unchanged by TARP γ-8 KO but up-regulated by MPH, or DEPs up-regulated or unchanged by TARP γ-8 KO but down-regulated by MPH). Consequently, the total number of DEPs from cortical synaptosomes declined from 114 to 111 (Supplementary Table S4), including 84 up-regulated and 27 down-regulated proteins.

Based on the 111 MPH-positive DEPs, KEGG pathway analysis identified a total of 16 enriched pathways (Figure 5C). The morphine addiction (P=1.93×10^{-4}) and estrogen signaling pathways (P=2.47×10^{-4}) were significantly enriched (P<0.001). Retrograde endocannabinoid signaling (P=2.96×10^{-3}), cholinergic synapses (P=4.14×10^{-3}), glutamatergic synapses (P=4.40×10^{-3}), dopaminergic synapses (P=7.55×10^{-3}), Parkinson's disease (P=1.08×10^{-2}), and GABAergic synapses (P=1.40×10^{-2}) were similarly significantly enriched (P<0.05). These results suggest that MPH has comprehensive effects on synaptic transmission regulation. Figure 5D shows the heat map of synapse-related DEPs with GO enrichment analysis. From cellular component analysis, 26 MPH-positive DEPs were mainly located in the dendrites, synapses, presynaptic membranes, neuronal cell bodies, postsynaptic densities, and myelin sheaths (Figure 5D, green lines). Biological process analysis revealed that these DEPs are associated with multiple functions, e.g., Grik2 (Figure 5D, blue lines) and Slc6a3 (Figure 5D, red lines) are associated with transport, aging, protein binding, and PDZ domain binding functions. In addition, Slc6a3, which is the protein that responds to ADHD medications, was naturally down-regulated by MPH in the cortical synaptosomes, which may explain the underlying mechanism by which adolescent TARP γ-8 KO mice respond to therapeutic drugs.

As shown in Figure 6A, DEPs in TARP γ-8 KO mice and after MPH treatment were analyzed in the prefrontal cortex. We established protein-protein interaction networks using the STRING database and visualized the networks using Cytoscape to gain a better understanding of the potential interactions among these DEPs. Twenty-three DEPs (red nodes) overlapped, indicating that the altered proteins induced by TARP γ-8 KO were reversed by MPH treatment. The connections between proteins were dense and complex. DEPs induced by TARP γ-8 KO and MPH treatment were functionally classified using the BiNGO plug-in in Cytoscape. Results revealed overlapping functional categories (Figure 6A). In particular, the functional categories of locomotory behavior, behavior, and synaptic transmission may be related to the occurrence of ADHD, which is characterized by behavioral dysfunction. By analyzing these functional categories, we identified a cluster (Figure 6B, red lines connecting proteins) related to the glutamatergic and dopaminergic pathways. In TARP γ-8 KO mice, the expression levels of Grik2, Th, and Slc6a3 were markedly up-regulated. However, Slc6a3 was inhibited by MPH and, similarly, the expression levels of Pick1 and Grik2 were down-regulated (Figure 6B, C). Considering that Slc6a3 modulates dopamine function (Madras et al., 2005) and Grik2 regulates glutamate function in synapses (Shaltiel et al., 2008), our findings indicate a potential inter-relationship between glutamatergic and dopaminergic pathways in prefrontal cortical synaptosomes.

Bioinformatic analysis of DEPs induced by MPH treatment in hippocampal synaptosomes

In total, 43 MPH-positive DEPs were identified in the hippocampal synaptosomes treated with MPH, including 39 up-regulated and four down-regulated proteins (Supplementary Table S5). Cellular component analysis

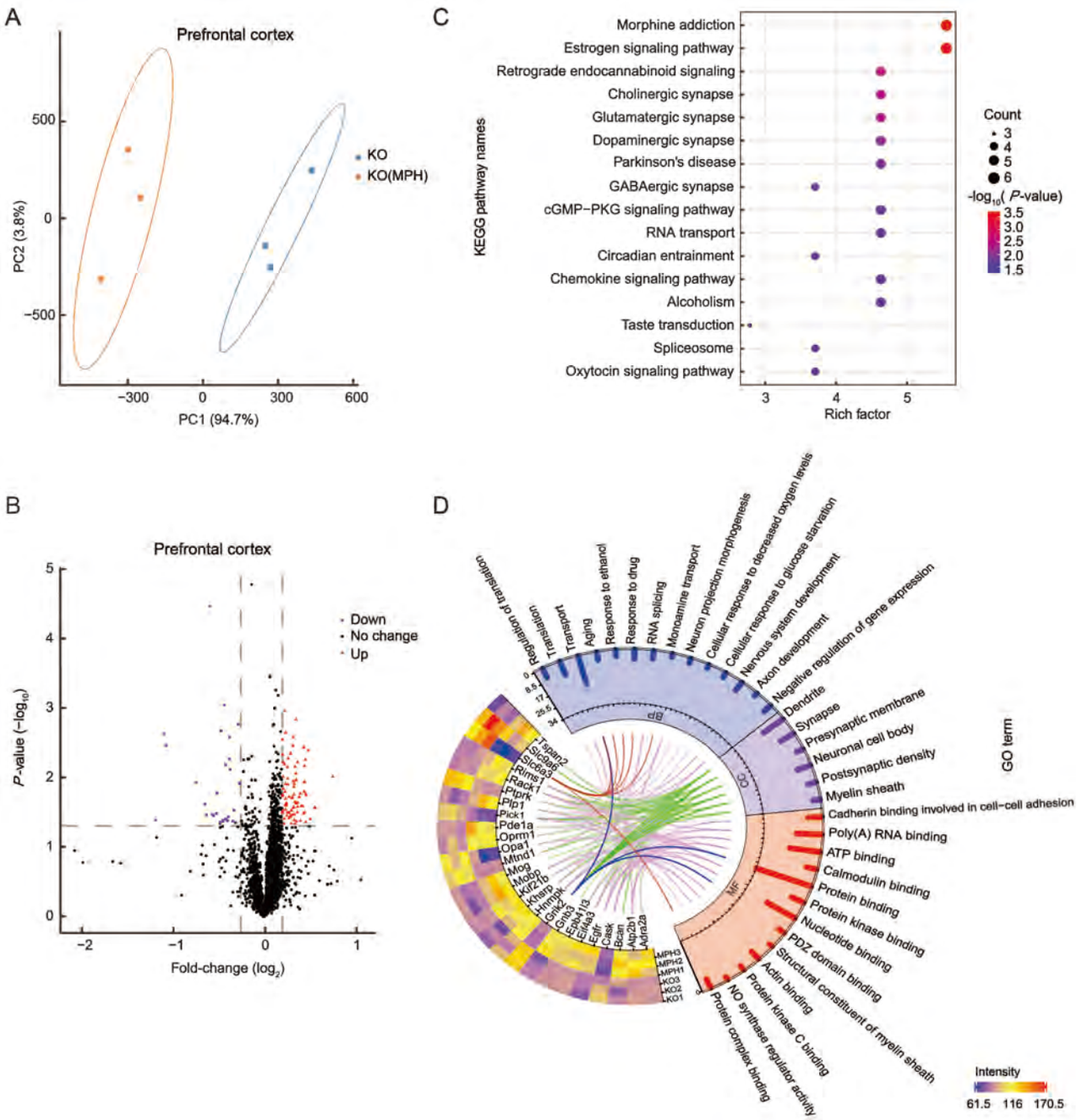

Figure 5 Proteomic analysis of identified proteins and DEPs in prefrontal cortical synaptosomes of TARP γ-8 KO mice after MPH treatment

A: PLS-DA of identified proteins from prefrontal cortical synaptosomes induced by MPH. KO (MPH) represents MPH-treated KO mice (orange), with saline-treated KO mice used for comparison (blue). B: Volcano plots of identified proteins from prefrontal cortical synaptosomes. Up-regulated proteins (red points) represents fold-change≥1.2 and P<0.05, down-regulated proteins (blue points) represent fold-change≤0.8 and P<0.05. C: Bubble chart of enriched KEGG pathways in DEPs induced by MPH in prefrontal cortical synaptosomes. X-axis represents Rich factor, with larger values indicating greater proportions of DEPs annotated to pathway. Y-axis represents KEGG pathway annotation entries. Dot size represents count of DEPs annotated to pathway. Dot color represents statistical significance of enriched KEGG pathway ($-\log_{10}P$-value), blue is lowest and red is highest significance. D: Heat map of synapse-related DEPs with GO enrichment analysis. Color scale of heat map indicates abundance of DEPs, blue is lowest and red is highest. GO enrichment analysis of biological processes (BP), cellular components (CC), and molecular functions (MF) of synapse-related DEPs. Bar plot indicates count of DEPs. For each category, P<0.05 was defined as significant. GO terms are sorted clockwise according to significance.

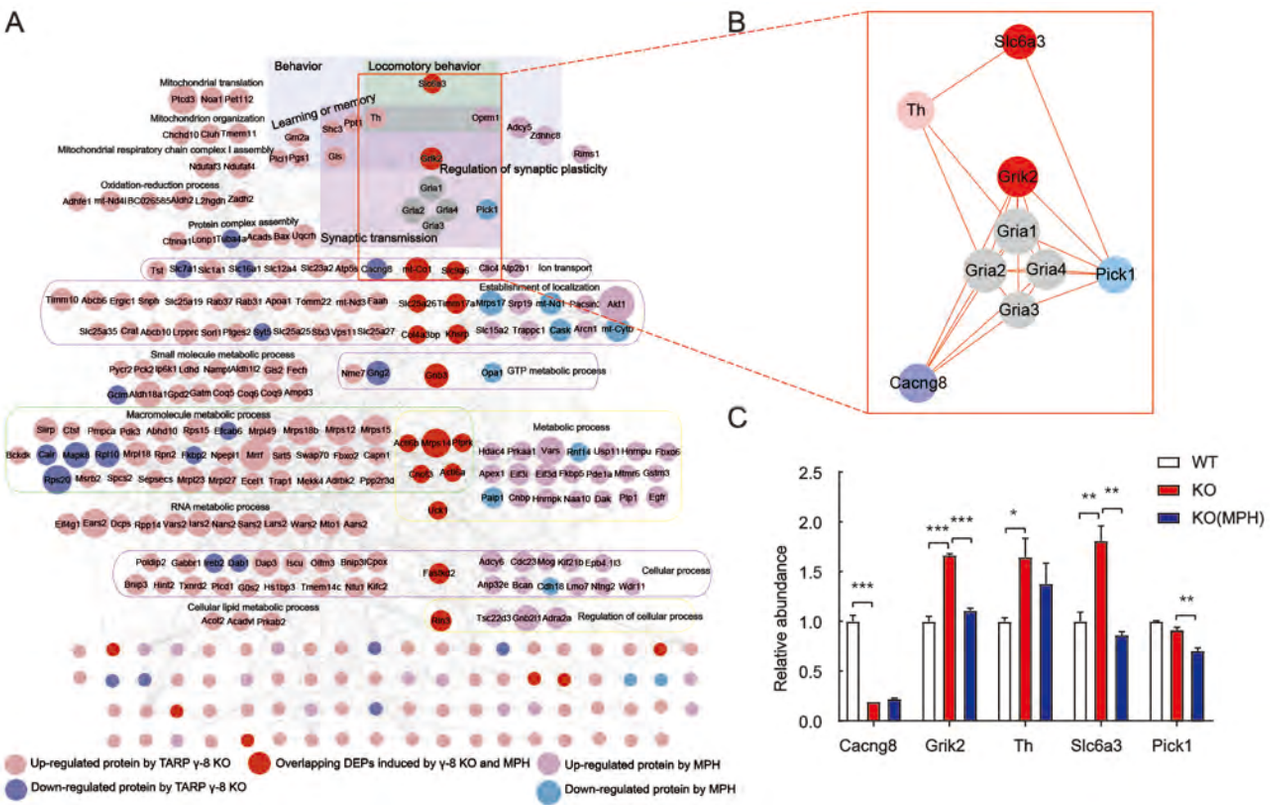

Figure 6 Construction of interaction networks of total DEPs in prefrontal cortical synaptosomes subjected to TARP γ-8 KO and MPH treatment

A: Protein-protein interaction network was constructed using the STRING database and Cytoscape software. Proteins in the network are shown as nodes, with size of nodes representing node degree (number of linked edges). Color of nodes represents up- or down-regulated proteins. For DEPs induced by TARP γ-8, up-regulated proteins are in lightpink and down-regulated proteins are in royalblue. For DEPs induced by MPH treatment, up-regulated proteins are in violet and down-regulated proteins are in skyblue. Red nodes represent overlap of DEPs induced by γ-8 and MPH. Gray nodes represent unaltered proteins. Width of lines connecting proteins indicates combined score given by the database. Different clusters of interacting proteins were analyzed using BiNGO, with some DEP clusters marked with different colored frames (gray frame: behavior; green frame: locomotory behavior; purple frame: synaptic transmission). B: Network cluster formed between glutamatergic and dopaminergic pathways. When Cacng8 was down-regulated by TARP γ-8 KO, Grik2, Th, and Slc6a3 were simultaneously up-regulated. Pick1 and Grik2 were down-regulated when Slc6a3 was inhibited and down-regulated by MPH treatment. C: Relative abundance of Cacng8, Grik2, Th, Slc6a3, and Pick1 from WT, TARP γ-8 KO, and TARP γ-8 KO (MPH) groups. All data are presented as means±*SEM*. Student's *t*-test was used, *: $P<0.05$; **: $P<0.01$; ***: $P<0.001$.

indicated that only 11 MPH-positive DEPs were located in the synaptic constitution based on their GO annotations (Figure 7C, green lines). Interestingly, Cnih2 and Porcn, associated auxiliary proteins of the AMPAR complex (Figure 7C, red line), were clearly identified (Figure 7C). As mentioned previously (Figure 3C, D), TARP γ-8 KO caused a large change in hippocampal AMPAR proteomes; however, MPH seemed to have less of an impact. To further clarify changes in the AMPAR complex, we used a heat map (Figure 7D) to illustrate the abundance of most constituents of the AMPARs in hippocampal synaptosomes from the WT, KO, and MPH treatment groups. As shown in Figure 7D, pore-forming Gria1–4 were significantly down-regulated following TARP γ-8 KO, but were not altered by MPH treatment. Moreover, most regulated proteins were not altered by MPH, including receptor core proteins (Cacng2, Cacng3, and Gsg1l) and peripheral proteins (Shisa6, Noelin, Cpt1c, and Abhd6). In line with previous research (Kato et al., 2010), Cnih-2 protein levels were markedly diminished in TARP γ-8 KO hippocampi. Interestingly, MPH obviously rescued Cnih-2 expression. In addition, Porcn, which was not altered in TARP γ-8 KO hippocampi, was markedly up-regulated after MPH treatment (Figure 7D).

MPH improved synaptic AMPAR function in hippocampal neurons of adolescent TARP γ-8 KO mice

Hippocampal AMPARs play key roles in learning and memory (Medin et al., 2019; Park et al., 2016). As mentioned above, MPH rescued impaired memory in TARP γ-8 KO mice under contextual fear conditioning. In contrast, total protein expression of hippocampal AMPARs was unaltered in TARP γ-8 KO mice treated with MPH. Cnih2, a positively regulated AMPAR auxiliary protein (Herring et al., 2013), and Porcn, a negatively regulated auxiliary protein (Wei et al., 2020), were both up-regulated after MPH treatment. Considering whether the hippocampal AMPAR function was altered in TARP γ-8 KO mice treated with MPH, we next investigated the effects of

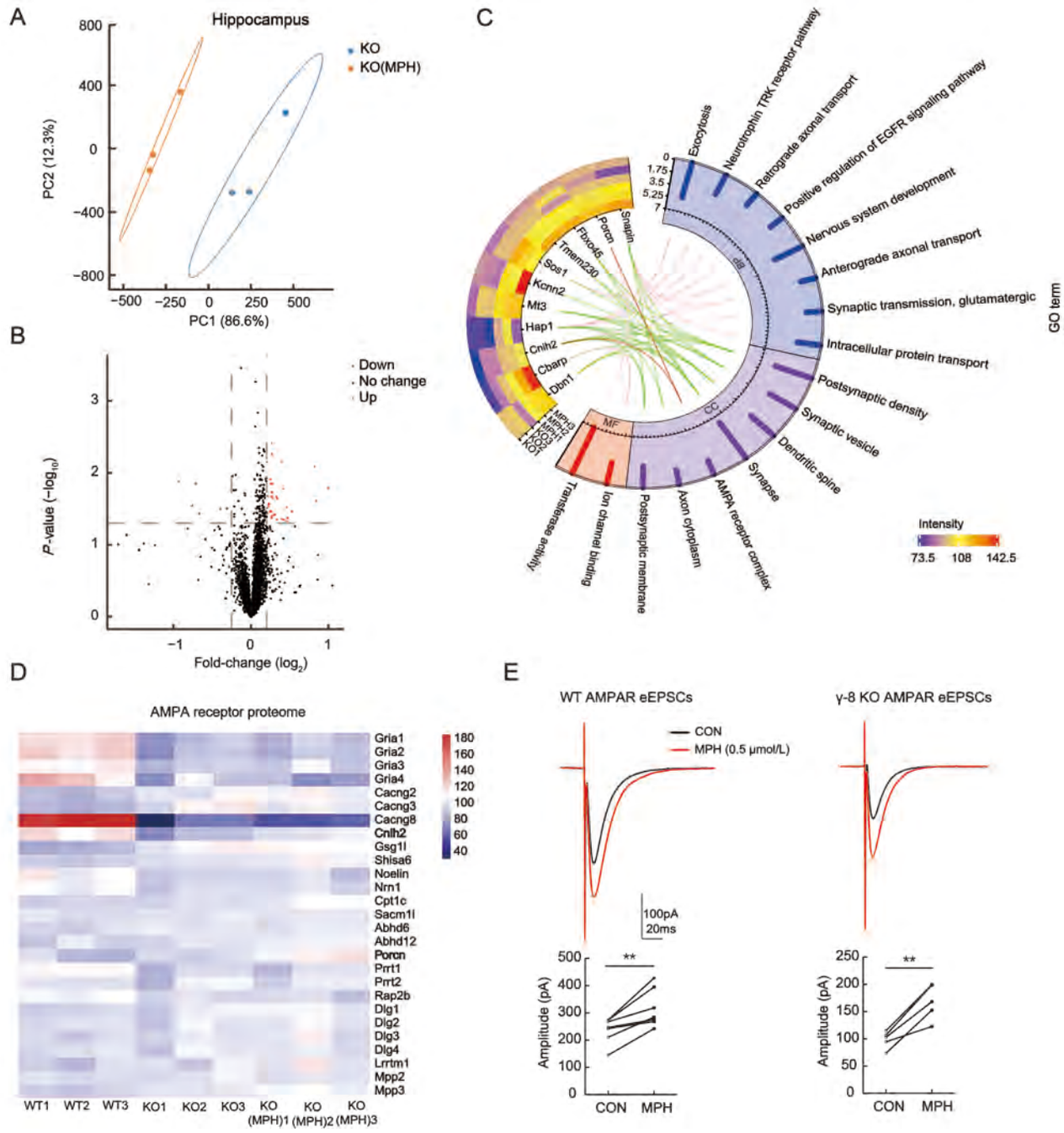

Figure 7 Proteomic analyses of hippocampal synaptosomes and functional modulation of AMPARs by MPH treatment

A: PLS-DA of identified proteins from hippocampal synaptosomes induced by MPH. B: Volcano plots of identified proteins from hippocampal synaptosomes. C: Heat map of synapse-related DEPs induced by MPH with GO enrichment analysis. D: Heat map of AMPAR proteome in hippocampal synaptosomes. Color scale of heat map indicates abundance of identified proteins, blue is lowest and red is highest. E: MPH (0.5 μmol/L) increased AMPAR-mediated synaptic transmission in hippocampal CA1 pyramidal neurons. Amplitude of AMPAR eEPSCs in WT (left) and TARP γ-8 KO mice (right) was significantly increased by MPH 0.5 μmol/L treatment, respectively. Seven cells from four mice in WT group and five cells from four mice in TARP γ-8 KO group. All data are presented as means±*SEM*. Paired *t*-test was used, *: $P<0.05$; **: $P<0.01$; ***: $P<0.001$.

MPH on hippocampal eEPSCs. Previous studies have indicated that AMPAR-mediated synaptic transmission is impaired in TARP γ-8 KO mice (Peng et al., 2021; Rouach et al., 2005). AMPAR eEPSC amplitude in the TARP γ-8 KO slices increased significantly from −98.7±7.0 pA to −168.4±14.5 pA (five cells from four mice; $P<0.01$) in response to MPH (0.5 μmol/L) treatment (Figure 7E) (Jenson et al., 2015). Similarly, MPH (0.5 μmol/L) increased AMPAR eEPSC amplitude in WT slices from −237.2±17.5 pA to −315.9±26.3 pA (seven cells from four mice; $P<0.01$)

(Figure 7E). These findings suggest that MPH improves synaptic AMPAR function in the hippocampal neurons of TARP γ-8 KO mice.

DISCUSSION

In the present study, we provide evidence for an association between TARP γ-8 and ADHD development. Notably, TARP γ-8 deficiency in adolescent mice led to a canonical ADHD-like phenotype with hyperactivity, impulsivity, anxiety, and cognitive and memory impairment, mimicking the clinical core symptoms and comorbidities of ADHD (Faraone et al., 2015; Thapar & Cooper, 2016). The synaptosomal proteomes revealed dopaminergic and glutamatergic transmission dysregulation in the prefrontal cortex and AMPA glutamate receptor complex dysfunction in the hippocampus of adolescent TARP γ-8 KO mice. Moreover, the major ADHD-like symptoms and altered synaptosomal proteins in TARP γ-8 KO mice were rescued by the key ADHD-drug MPH, which is often used in other ADHD animal models (Li et al, 2017; Won et al, 2011). These findings suggest that adolescent TARP γ-8 KO mice may serve as a murine model of ADHD as they fit the criteria (facial, constructal, and predictive validity) for ADHD animal models (De La Peña et al., 2018).

Previous study has indicated that TARP γ-8 deficiency in adult mice can lead to behavioral characteristics linked to antisocial personality disorder (ASPD) (Peng et al., 2021), indicating overlapping pathogenesis in both psychiatric disorders. In addition, children with ADHD are more likely to develop ASPD or other psychological disorders later in life (Storebø & Simonsen, 2016). Our large-scale phenome-wide association analysis demonstrated that among the 14 neuropsychiatric disorders examined, the *CACNG8* variants were most significantly associated with ADHD. These associations were replicable in several independent cohorts across ADHD, Parkinson's disease, multiple sclerosis, and schizophrenia in the same effect direction, as well as major depression in the opposite effect direction, indicating that a common pathogenesis related to *CACNG8* may be shared by these neuropsychiatric disorders. Consistent with previous research (Guan et al., 2016), two SNPs, i.e., rs11084307 and rs10420331, in the intronic region of *CACNG8* were also significantly associated with schizophrenia. Current research indicates that both ADHD and schizophrenia are related to neurodevelopmental disorders (Gudmundsson et al., 2019) and share overlapping alleles (Hamshere et al., 2013). Due to their similar physiopathological features, childhood ADHD is associated with an increased risk of subsequent schizophrenia (Nourredine et al., 2021). Our results showed that the most significant ADHD risk variant, rs11084307, together with closely linked rs10420331, was biologically functional. The ADHD risk alleles significantly increased cortical surface area (SA) of the insula and decreased cortical thickness (TH) of the pars triangularis. The insula is believed to play roles in diverse functions, including attention (Craig, 2009). In particular, the right anterior insula is associated with attention problems and inhibition, which are core symptoms of ADHD (Lopez-Larson et al., 2012), whereas the right posterior insula increases with ADHD symptom severity (Geurts et al., 2013), thus supporting our findings. Furthermore, children with ADHD have shorter right pars triangularis than children without ADHD, and right anterior ascending ramus length is related to attention problems in ADHD (Kibby et al., 2009), thus also supporting our findings.

In view of the complexity and heterogeneity of ADHD (Posner et al., 2020), its exact neuropathophysiology remains unclear. Recently, the prefrontal cortex (Arnsten, 2009) and hippocampus (Al-Amin et al., 2018) have emerged as the primary brain regions showing deficits in ADHD. The prefrontal cortex is connected to key subcortical regions that form a network of neurons for regulating attention, motor responses, working memory, and emotions (Arnsten, 2009; Biederman, 2005; Faraone et al., 2015). The hippocampus plays a critical role in memory acquisition, consolidation, and retrieval (Abel & Lattal, 2001). Studies have found that hippocampal volume reduction (Hoogman et al., 2017) and connections with other brain regions are dysfunctional in children with ADHD (Posner et al., 2014). Increasing evidence indicates that synaptic catecholaminergic (Arnsten, 2009; Arnsten & Pliszka, 2011; Prince, 2008) and glutamatergic transmission dysfunction (Cheng et al., 2017; Miller et al., 2014) occur in the prefrontal cortex in ADHD. Dysregulation of hippocampal synaptic transmission, especially disruption of glutamatergic transmission, contributes to the abnormal behavioral symptoms in people with ADHD (Medin et al., 2019). These findings are consistent with our synaptosomal proteomic results for TARP γ-8 KO mice, whereby synaptic transmission dysregulation primarily occurred in the dopaminergic and glutamatergic synapses of the prefrontal cortex and AMPAR complex of the hippocampus.

We identified 265 DEPs from cortical synaptosomes associated with 11 biological pathways in TARP γ-8 KO mice (Figure 2D). Of the synapse-associated pathways, those that were significantly enriched included the GABAergic, glutamatergic, and dopaminergic synaptic pathways, which are closely associated with ADHD (Cheng et al., 2017; Del Campo et al., 2011; Solleveld et al., 2017). To further explore the biological mechanisms of the ADHD-like model in prefrontal cortical synaptosomes, we constructed protein-protein interaction networks (Figure 6A, B). Interestingly, we found a network cluster reflecting interactions between the glutamatergic and dopaminergic pathways, which are related to behavioral dysfunction in ADHD (Sagvolden et al., 2005). In this cluster, when Cacng8 was down-regulated by TARP γ-8 KO, Grik2, Th, and Slc6a3 were simultaneously up-regulated. Furthermore, Pick1 and Grik2 were down-regulated when Slc6a3 (target of ADHD) was inhibited and down-regulated by MPH treatment. These results provide evidence that the dopaminergic and glutamatergic pathways work synergistically and affect each other in TARP γ-8 KO mice.

Although the interaction mechanism of the network cluster in the prefrontal cortex remains unclear, Slc6a3 and Grik2 may play important roles in ADHD-like behaviors. This observation is consistent with the dynamic developmental behavioral theory of ADHD (Sagvolden et al., 2005): i.e., hypofunction of dopaminergic signals leads to inappropriate modulation of nondopaminergic signals, such as glutamatergic signal transmission (Prince, 2008; Sagvolden et al., 2005).

Slc6a3, which encodes sodium-dependent dopamine transporters, removes dopamine from the synaptic cleft and regulates dopamine availability in synapses (Madras et al., 2005). When Slc6a3 was inhibited and down-regulated after MPH treatment, the glutamatergic receptor Grik2 was correspondingly down-regulated. Likewise, with KO of the *CACNG8* gene from the glutamatergic pathway in model mice, Grik2 was significantly up-regulated, and Slc6a3 from the dopaminergic pathway was also significantly up-regulated. As TARP γ-8 is an auxiliary subunit of AMPARs, AMPAR-deficient mice also display ADHD-like behavior (Aitta-Aho et al., 2019) and spontaneously hypertensive rats manifest AMPAR dysfunction in the prefrontal cortex (Cheng et al., 2017) and hippocampus (Medin et al., 2019). Our results suggest a supplementary theory that abnormal glutamatergic transmission also leads to improper regulation of dopaminergic transmission in the prefrontal cortex in ADHD. Furthermore, Grik2 is reported to be involved in several behavioral disorders, although findings are inconsistent. For example, *Grik2* KO mice are hyperactive and hyper-responsive to stimulants in models of mania (Shaltiel et al., 2008), deletion of the *Grik2* gene reduces locomotor activity and sociability in autism (Micheau et al., 2014), and blocking Gluk2 receptors attenuates sevoflurane-induced hyperactivity (Liang et al., 2017). Here, Grik2 was obviously up-regulated in the TARP γ-8 KO ADHD-like model; however, the underlying mechanism of this action needs to be further studied.

TARP γ-8 is preferentially expressed in the hippocampus (Tomita et al., 2003), controls basal AMPAR expression and localization at extrasynaptic sites (Rouach et al., 2005), and is involved in the dynamic-state mobilization of AMPARs to synaptic sites to regulate synaptic transmission and plasticity (Sumioka et al., 2011). TARP γ-8 also plays a critical role in long-term potentiation, learning, and memory (Park et al., 2016). Proteomic analysis of hippocampal synaptosomes revealed that the glutamatergic synaptic pathway was significantly enriched (Figure 3C). We performed bioinformatic analysis to explore changes in the AMPA glutamate receptor complex in TARP γ-8 KO mice. Following the down-regulation of Cacng8, we observed changes in many core proteins associated with the biological processes of AMPAR activity, including proteins regulating synaptic transmission and neuronal synaptic plasticity (Figure 3D). These findings are consistent with previously reported changes in AMPAR function and expression in animal models of ADHD (Cheng et al., 2017; Medin et al., 2019). However, MPH appeared to have little effect on the expression of these proteins, with the exception of regulatory proteins Cnih-2 and Porcn (Figure 7D). These results suggest that MPH may act primarily in the prefrontal cortex to treat ADHD, as well as modulate the function of hippocampal synapses.

Cnih2, an additional AMPAR auxiliary subunit, promotes surface trafficking and enhances AMPAR gating (Schwenk et al., 2009). Previous studies have found that both TARP γ-8 and Cnih2 are associated with postsynaptic densities, and Cnih2 expression is markedly diminished in TARP γ-8 KO mice (Kato et al., 2010). This finding is consistent with our results showing that Cnih2 proteins were significantly down-regulated in adolescent TARP γ-8 KO mice. Furthermore, these results indicate a sophisticated interaction between TARP γ-8 and Cnih2 (Herring et al., 2013; Kato et al., 2010). Previous studies have suggested that Cnih2 may displace TARP γ-8 and occupy TARP γ-8 binding sites on AMPARs (Gill et al., 2011; Herring et al., 2013). This may partly explain our finding that Cnih2 was up-regulated after MPH treatment in the TARP γ-8 KO synaptosomes. Porcn, a transmembrane protein associated with AMPAR (Erlenhardt et al., 2016), is located at the periphery of the AMPAR complex (Brechet et al., 2017). Several studies have found that down-regulation of Porcn selectively reduces AMPAR levels and basal synaptic transmission (Erlenhardt et al., 2016), whereas other studies have found that Porcn negatively regulates AMPAR trafficking to the plasma and inhibits glutamate-induced currents and AMPAR surface expression (Wei et al., 2020). Although the precise action of Porcn up-regulation in MPH treatment is unknown, MPH significantly increased the amplitude of AMPAR eEPSCs in TARP γ-8 KO slices following up-regulation of Cnih2 and Porcn in our study. These findings are consistent with recent reports that MPH enhances the function of AMPAR in synapses (Rozas et al., 2015). These results may be due to the synergistic effects of additional AMPAR auxiliary regulatory proteins, although the specific mechanisms require further study.

In conclusion, we identified an association between TARP γ-8 and ADHD development. Synaptosomal proteomic analysis confirmed significant changes in the protein expression levels in the dopaminergic and glutamatergic systems and in the interactions between the two pathways. Human phenome-wide association study further identified significant associations between CACNG8 variants and ADHD. Based on these findings, our results indicate that TARP γ-8 KO, which primarily disrupts glutamatergic transmission, can lead to ADHD-like pathogenesis, distinct from the theory of catecholamine signaling dysregulation. This model should facilitate our understanding of the glutamatergic pathway in ADHD pathogenesis and provide novel insights into the mechanisms underlying ADHD.

DATA AVAILABILITY

The datasets used for analyses described in this manuscript were obtained from dbGaP (https://www.ncbi.nlm.nih.gov/gap/). The dbGaP accession numbers are listed in Supplementary Table S1.

SUPPLEMENTARY DATA

Supplementary data to this article can be found online.

COMPETING INTERESTS

The authors declare that they have no competing interests.

AUTHORS' CONTRIBUTIONS

The authors contributed as follows: W.Z., D.Z.K., and W.J.B. designed the research and prepared the manuscript; W.J.B., B.H.J., K.S.Z., W.Y.G., and X.Q.Z. performed the experiments; W.J.B., X.Q., Z.X.Y., J.J.Z., S.R.C., R.W., and J.H. analyzed the data; Y.S.S. provided professional guidance

for experiment design and TARP γ-8 gene heterozygous breeding mice. X.G.L. and F.W. performed phenome-wide association study and prepared the related manuscript. All authors read and approved the final version of the manuscript.

ACKNOWLEDGMENTS

We thank the NIH GWAS Data Repository, contributing investigators who provided phenotypic and genotypic data from their original study, and primary funding organizations that supported the contributing studies. Funding and other support of phenotypic and genotypic data were provided through the National Institutes of Health (NIH) and other agencies.

REFERENCES

Abel T, Lattal KM. 2001. Molecular mechanisms of memory acquisition, consolidation and retrieval. *Current Opinion in Neurobiology*, **11**(2): 180−187.

Adler LA, Kroon RA, Stein M, Shahid M, Tarazi FI, Szegedi A, et al. 2012. A translational approach to evaluate the efficacy and safety of the novel AMPA receptor positive allosteric modulator org 26576 in adult attention-deficit/hyperactivity disorder. *Biological Psychiatry*, **72**(11): 971−977.

Aitta-Aho T, Maksimovic M, Dahl K, Sprengel R, Korpi ER. 2019. Attenuation of novelty-induced hyperactivity of gria1-/- mice by Cannabidiol and hippocampal inhibitory Chemogenetics. *Frontiers in Pharmacology*, **10**: 309.

Al-Amin M, Zinchenko A, Geyer T. 2018. Hippocampal subfield volume changes in subtypes of attention deficit hyperactivity disorder. *Brain Research*, **1685**: 1−8.

Arnsten AFT. 2009. Toward a new understanding of attention-deficit hyperactivity disorder pathophysiology: an important role for prefrontal cortex dysfunction. *CNS Drugs*, **23**(S1): 33−41.

Arnsten AFT, Pliszka SR. 2011. Catecholamine influences on prefrontal cortical function: relevance to treatment of attention deficit/hyperactivity disorder and related disorders. *Pharmacology Biochemistry and Behavior*, **99**(2): 211−216.

Barker GRI, Bird F, Alexander V, Warburton EC. 2007. Recognition memory for objects, place, and temporal order: a disconnection analysis of the role of the medial prefrontal cortex and perirhinal cortex. *Journal of Neuroscience*, **27**(11): 2948−2957.

Bauer J, Werner A, Kohl W, Kugel H, Shushakova A, Pedersen A, et al. 2018. Hyperactivity and impulsivity in adult attention-deficit/hyperactivity disorder is related to glutamatergic dysfunction in the anterior cingulate cortex. *The World Journal of Biological Psychiatry*, **19**(7): 538−546.

Biederman J. 2005. Attention-deficit/hyperactivity disorder: a selective overview. *Biological Psychiatry*, **57**(11): 1215−1220.

Bouchatta O, Manouze H, Bouali-Benazzouz R, Kerekes N, Ba-M'hamed S, Fossat P, et al. 2018. Neonatal 6-OHDA lesion model in mouse induces Attention-Deficit/ Hyperactivity Disorder (ADHD)-like behaviour. *Scientific Reports*, **8**(1): 15349.

Brechet A, Buchert R, Schwenk J, Boudkkazi S, Zolles G, Siquier-Pernet K, et al. 2017. AMPA-receptor specific biogenesis complexes control synaptic transmission and intellectual ability. *Nature Communications*, **8**(1): 15910.

Calzavara MB, Medrano WA, Levin R, Kameda SR, Andersen ML, Tufik S, et al. 2009. Neuroleptic drugs revert the contextual fear conditioning deficit presented by spontaneously hypertensive rats: a potential animal model of emotional context processing in schizophrenia?. *Schizophrenia Bulletin*, **35**(4): 748−759.

Chen XJ, Zhang WG, Li T, Guo Y, Tian YP, Wang F, et al. 2015. Impairment of oligodendroglia maturation leads to aberrantly increased cortical glutamate and anxiety-like behaviors in juvenile mice. *Frontiers in Cellular Neuroscience*, **9**: 467.

Cheng J, Liu AY, Shi MY, Yan Z. 2017. Disrupted glutamatergic transmission in prefrontal cortex contributes to behavioral abnormality in an animal model of ADHD. *Neuropsychopharmacology*, **42**(10): 2096−2104.

Craig AD. 2009. Emotional moments across time: a possible neural basis for time perception in the anterior insula. *Philosophical Transactions of the Royal Society B Biological Sciences*, **364**(1525): 1933−1942.

De La Peña JB, Dela Peña IJ, Custodio RJ, Botanas CJ, Kim HJ, Cheong JH. 2018. Exploring the validity of proposed transgenic animal models of attention-deficit hyperactivity disorder (ADHD). *Molecular Neurobiology*, **55**(5): 3739−3754.

Del Campo N, Chamberlain SR, Sahakian BJ, Robbins TW. 2011. The roles of dopamine and noradrenaline in the pathophysiology and treatment of attention-deficit/hyperactivity disorder. *Biological Psychiatry*, **69**(12): e145−e157.

Erlenhardt N, Yu H, Abiraman K, Yamasaki T, Wadiche JI, Tomita S, et al. 2016. Porcupine controls hippocampal AMPAR levels, composition, and synaptic transmission. *Cell Reports*, **14**(4): 782−794.

Faraone SV, Asherson P, Banaschewski T, Biederman J, Buitelaar JK, Ramos-Quiroga JA, et al. 2015. Attention-deficit/hyperactivity disorder. *Nature Reviews Disease Primers*, **1**: 15020.

Fukaya M, Tsujita M, Yamazaki M, Kushiya E, Abe M, Akashi K, et al. 2006. Abundant distribution of TARP γ-8 in synaptic and extrasynaptic surface of hippocampal neurons and its major role in AMPA receptor expression on spines and dendrites. *European Journal of Neuroscience*, **24**(8): 2177−2190.

Geurts HM, Ridderinkhof KR, Scholte HS. 2013. The relationship between grey-matter and ASD and ADHD traits in typical adults. *Journal of Autism and Developmental Disorders*, **43**(7): 1630−1641.

Gill MB, Kato AS, Roberts MF, Yu H, Wang H, Tomita S, et al. 2011. Cornichon-2 modulates AMPA receptor-transmembrane AMPA receptor regulatory protein assembly to dictate gating and pharmacology. *Journal of Neuroscience*, **31**(18): 6928−6938.

Gleason SD, Kato A, Bui HH, Thompson LK, Valli SN, Stutz PV, et al. 2015. Inquiries into the biological significance of transmembrane AMPA receptor regulatory protein (TARP) γ-8 through investigations of TARP γ-8 null mice§. *CNS & Neurological Disorders-Drug Targets*, **14**(5): 612−626.

Guan FL, Zhang TX, Liu XS, Han W, Lin HL, Li L, et al. 2016. Evaluation of voltage-dependent calcium channel γ gene families identified several novel potential susceptible genes to schizophrenia. *Scientific Reports*, **6**: 24914.

Gudmundsson OO, Walters GB, Ingason A, Johansson S, Zayats T, Athanasiu L, et al. 2019. Attention-deficit hyperactivity disorder shares copy number variant risk with schizophrenia and autism spectrum disorder. *Translational Psychiatry*, **9**(1): 258.

Hamshere ML, Stergiakouli E, Langley K, Martin J, Holmans P, Kent L, et al. 2013. Shared polygenic contribution between childhood attention-deficit hyperactivity disorder and adult schizophrenia. *British Journal of Psychiatry*, **203**(2): 107−111.

Herring BE, Shi Y, Suh YH, Zheng CY, Blankenship SM, Roche KW, et al. 2013. Cornichon proteins determine the subunit composition of synaptic AMPA receptors. *Neuron*, **77**(6): 1083−1096.

Hoogman M, Bralten J, Hibar DP, Mennes M, Zwiers MP, Schweren LSJ, et al. 2017. Subcortical brain volume differences in participants with attention deficit hyperactivity disorder in children and adults: a cross-sectional mega-analysis. *The Lancet Psychiatry*, **4**(4): 310−319.

Jenson D, Yang KC, Acevedo-Rodriguez A, Levine A, Broussard JI, Tang JR, et al. 2015. Dopamine and norepinephrine receptors participate in methylphenidate enhancement of *in vivo* hippocampal synaptic plasticity. *Neuropharmacology*, **90**: 23−32.

Kato AS, Gill MB, Ho MT, Yu H, Tu Y, Siuda ER, et al. 2010. Hippocampal AMPA receptor gating controlled by both TARP and cornichon proteins. *Neuron*, **68**(6): 1082−1096.

Kibby MY, Kroese JM, Krebbs H, Hill CE, Hynd GW. 2009. The pars triangularis in dyslexia and ADHD: A comprehensive approach. *Brain and Language*, **111**(1): 46−54.

Kong DZ, Tian XL, Li YS, Zhang SH, Cheng YR, Huo LF, et al. 2018. Revealing the Inhibitory Effect of Ginseng on Mitochondrial Respiration through Synaptosomal Proteomics. *Proteomics*, **18**(11): 1700354.

Kotecha SA, Oak JN, Jackson MF, Perez Y, Orser BA, Van Tol HHM, et al. 2002. A D2 class dopamine receptor transactivates a receptor tyrosine kinase to inhibit NMDA receptor transmission. *Neuron*, **35**(6): 1111−1122.

Li Y, Yin AQ, Sun X, Zhang M, Zhang JF, Wang P, et al. 2017. Deficiency of tumor suppressor NDRG2 leads to attention deficit and hyperactive behavior. *The Journal of Clinical Investigation*, **127**(12): 4270−4284.

Liang P, Li F, Liu J, Liao D, Huang H, Zhou C. 2017. Sevoflurane activates hippocampal CA3 kainate receptors (Gluk2) to induce hyperactivity during induction and recovery in a mouse model. *British Journal of Anaesthesia*, **119**(5): 1047−1054.

Lopez-Larson MP, King JB, Terry J, McGlade EC, Yurgelun-Todd D. 2012. Reduced insular volume in attention deficit hyperactivity disorder. *Psychiatry Research:Neuroimaging*, **204**(1): 32−39.

Madras BK, Miller GM, Fischman AJ. 2005. The dopamine transporter and attention-deficit/hyperactivity disorder. *Biological Psychiatry*, **57**(11): 1397−1409.

Matsuoka Y, Furuyashiki T, Yamada K, Nagai T, Bito H, Tanaka Y, et al. 2005. Prostaglandin E receptor EP1 controls impulsive behavior under stress. *Proceedings of the National Academy of Sciences of the United States of America*, **102**(44): 16066−16071.

Medin T, Jensen V, Skare Ø, Storm-Mathisen J, Hvalby Ø, Bergersen LH. 2019. Altered α-amino-3-hydroxy-5-methyl-4-isoxazolepropionic acid (AMPA) receptor function and expression in hippocampus in a rat model of attention-deficit/hyperactivity disorder (ADHD). *Behavioural Brain Research*, **360**: 209−215.

Micheau J, Vimeney A, Normand E, Mulle C, Riedel G. 2014. Impaired hippocampus-dependent spatial flexibility and sociability represent autism-like phenotypes in GluK2 mice. *Hippocampus*, **24**(9): 1059−1069.

Miller EM, Pomerleau F, Huettl P, Gerhardt GA, Glaser PEA. 2014. Aberrant glutamate signaling in the prefrontal cortex and striatum of the spontaneously hypertensive rat model of attention-deficit/hyperactivity disorder. *Psychopharmacology*, **231**(15): 3019−3029.

Naaijen J, Bralten J, Poelmans G, The IMAGE Consortium, Glennon JC, Franke B, et al. 2017. Glutamatergic and GABAergic gene sets in attention-deficit/hyperactivity disorder: association to overlapping traits in ADHD and autism. *Translational Psychiatry*, **7**(1): e999.

NC3Rs Reporting Guidelines Working Group. 2010. Animal research: reporting *in vivo* experiments: the ARRIVE guidelines. *Experimental Physiology*, **95**(8): 842−844.

Nourredine M, Gering A, Fourneret P, Rolland B, Falissard B, Cucherat M, et al. 2021. Association of attention-deficit/hyperactivity disorder in childhood and adolescence with the risk of subsequent psychotic disorder: a systematic review and meta-analysis. *JAMA Psychiatry*, **78**(5): 519−529.

Park J, Chávez AE, Mineur YS, Morimoto-Tomita M, Lutzu S, Kim KS, et al. 2016. CaMKII phosphorylation of TARPγ-8 is a mediator of LTP and learning and memory. *Neuron*, **92**(1): 75−83.

Peng SX, Wang YY, Zhang M, Zang YY, Wu D, Pei JW, et al. 2021. SNP rs10420324 in the AMPA receptor auxiliary subunit TARP γ-8 regulates the susceptibility to antisocial personality disorder. *Scientific Reports*, **11**(1): 11997.

Polanczyk G, De Lima MS, Horta BL, Biederman J, Rohde LA. 2007. The worldwide prevalence of ADHD: a systematic review and metaregression analysis. *The American Journal of Psychiatry*, **164**(6): 942−948.

Posner J, Polanczyk GV, Sonuga-Barke E. 2020. Attention-deficit hyperactivity disorder. *The Lancet*, **395**(10222): 450−462.

Posner J, Siciliano F, Wang ZS, Liu J, Sonuga-Barke E, Greenhill L. 2014. A multimodal MRI study of the hippocampus in medication-naive children with ADHD: what connects ADHD and depression?. *Psychiatry Research:Neuroimaging*, **224**(2): 112−118.

Pozzi M, Carnovale C, Mazhar F, Peeters GGAM, Gentili M, Nobile M, et al. 2019. Adverse drug reactions related to mood and emotion in pediatric patients treated for attention deficit/hyperactivity disorder: A comparative analysis of the US food and drug administration adverse event reporting system database. *Journal of Clinical Psychopharmacology*, **39**(4): 386−392.

Prince J. 2008. Catecholamine dysfunction in attention-deficit/hyperactivity disorder: an update. *Journal of Clinical Psychopharmacology*, **28**(3 Suppl 2): S39–S45.

Reisel D, Bannerman DM, Schmitt WB, Deacon RMJ, Flint J, Borchardt T, et al. 2002. Spatial memory dissociations in mice lacking GluR1. *Nature Neuroscience*, **5**(9): 868−873.

Reith MEA, Kortagere S, Wiers CE, Sun H, Kurian MA, Galli A, et al. 2022. The dopamine transporter gene *SLC6A3*: multidisease risks. *Molecular Psychiatry*, **27**(2): 1031−1046.

Rouach N, Byrd K, Petralia RS, Elias GM, Adesnik H, Tomita S, et al. 2005. TARP γ-8 controls hippocampal AMPA receptor number, distribution and synaptic plasticity. *Nature Neuroscience*, **8**(11): 1525−1533.

Rozas C, Carvallo C, Contreras D, Carreño M, Ugarte G, Delgado R, et al. 2015. Methylphenidate amplifies long-term potentiation in rat hippocampus CA1 area involving the insertion of AMPA receptors by activation of β-adrenergic and D1/D5 receptors. *Neuropharmacology*, **99**: 15−27.

Sagvolden T, Johansen EB, Aase H, Russell VA. 2005. A dynamic developmental theory of attention-deficit/hyperactivity disorder (ADHD) predominantly hyperactive/impulsive and combined subtypes. *Behavioral and Brain Sciences*, **28**(3): 397−419.

Schwenk J, Harmel N, Zolles G, Bildl W, Kulik A, Heimrich B, et al. 2009. Functional proteomics identify cornichon proteins as auxiliary subunits of AMPA receptors. *Science*, **323**(5919): 1313−1319.

Seibenhener ML, Wooten MC. 2015. Use of the open field maze to measure locomotor and anxiety-like behavior in mice. *Journal of Visualized Experiments*, (96): 52434.

Shaltiel G, Maeng S, Malkesman O, Pearson B, Schloesser RJ, Tragon T, et al. 2008. Evidence for the involvement of the Kainate receptor subunit GluR6 (GRIK2) in mediating behavioral displays related to behavioral symptoms of mania. *Molecular Psychiatry*, **13**(9): 858−872.

Sharma A, Couture J. 2013. A review of the pathophysiology, etiology, and

treatment of attention-deficit hyperactivity disorder (ADHD). *Annals of Pharmacotherapy*, **48**(2): 209−225.

Shaw P, Eckstrand K, Sharp W, Blumenthal J, Lerch JP, Greenstein D, et al. 2007. Attention-deficit/hyperactivity disorder is characterized by a delay in cortical maturation. *Proceedings of the National Academy of Sciences of the United States of America*, **104**(49): 19649−19654.

Solleveld MM, Schrantee A, Puts NAJ, Reneman L, Lucassen PJ. 2017. Age-dependent, lasting effects of methylphenidate on the GABAergic system of ADHD patients. *NeuroImage:Clinical*, **15**: 812−818.

Storebø OJ, Simonsen E. 2016. The association between ADHD and antisocial personality disorder (ASPD): A review. *Journal of Attention Disorders*, **20**(10): 815−824.

Sumioka A, Brown TE, Kato AS, Bredt DS, Kauer JA, Tomita S. 2011. PDZ binding of TARPγ-8 controls synaptic transmission but not synaptic plasticity. *Nature Neuroscience*, **14**(11): 1410−1412.

Thapar A, Cooper M. 2016. Attention deficit hyperactivity disorder. *The Lancet*, **387**(10024): 1240−1250.

Tomita S, Chen L, Kawasaki Y, Petralia RS, Wenthold RJ, Nicoll RA, et al. 2003. Functional studies and distribution define a family of transmembrane AMPA receptor regulatory proteins. *Journal of Cell Biology*, **161**(4): 805−816.

Wei MP, Wang M, Wang J, Su F, Wang YZ, Sun M, et al. 2020. PORCN negatively regulates AMPAR function independently of subunit composition and the amino-terminal and Carboxy-terminal domains of AMPARs. *Frontiers in Cell and Developmental Biology*, **8**: 829.

Witkin JM, Li J, Gilmour G, Mitchell SN, Carter G, Gleason SD, et al. 2017. Electroencephalographic, cognitive, and neurochemical effects of LY3130481 (CERC-611), a selective antagonist of TARP-γ8-associated AMPA receptors. *Neuropharmacology*, **126**: 257−270.

Won H, Mah W, Kim E, Kim JW, Hahm EK, Kim MH, et al. 2011. GIT1 is associated with ADHD in humans and ADHD-like behaviors in mice. *Nature Medicine*, **17**(5): 566−572.

Xu N, Zhou WJ, Wang Y, Huang SH, Li X, Chen ZY. 2015. Hippocampal Wnt3a is necessary and sufficient for contextual fear memory acquisition and consolidation. *Cerebral Cortex*, **25**(11): 4062−4075.

Yu YZ, Yang ZX, Jin BH, Qin X, Zhu XQ, Sun JH, et al. 2020. Cannabidiol inhibits febrile seizure by modulating AMPA receptor kinetics through its interaction with the N-terminal domain of GluA1/GluA2. *Pharmacological Research*, **161**: 105128.